



Cite this: *Mater. Adv.*, 2022, 3, 1849

Received 17th October 2021,  
Accepted 9th January 2022

DOI: 10.1039/d1ma00959a

[rsc.li/materials-advances](http://rsc.li/materials-advances)

Department of Chemistry and Biomolecular Science, Clarkson University, Potsdam, NY 13699, USA. E-mail: [ekatz@clarkson.edu](mailto:ekatz@clarkson.edu)

† Deceased in 2021.



**Daniel Massana Roquero**

alginic hydrogels. Daniel's study has resulted in various signal-triggered biomolecule release systems for biomedical and biotechnological applications.

## Iron(III)-cross-linked alginate hydrogels: a critical review

Daniel Massana Roquero, Ali Othman, Artem Melman † and Evgeny Katz \*

Ionotropic alginate hydrogels are versatile materials for a wide range of applications. Their biocompatibility and biodegradability have made them perfect candidates for biomedical applications such as tissue engineering and drug delivery. The vast majority of the research related to ionotropic alginate hydrogels has been conducted on  $\text{Ca}^{2+}$ -cross-linked alginate. However, alginate can produce hydrogels with a large number of divalent and trivalent cations. In recent years, the cross-linking of alginate with  $\text{Fe}^{3+}$  cations has attracted increasing interest due to its extraordinary properties. The particular coordination of  $\text{Fe}^{3+}$  cations has been found to be critical for mechanical strength, porosity, swelling and other physicochemical properties of the material rarely seen in other ionotropic alginate hydrogels. In addition, the rich redox chemistry of  $\text{Fe}^{3+}$  cations has been exploited for a wide range of applications, such as drug delivery, tissue engineering, or environmental remediation. In this review we highlight the state-of-the-art that concerns  $\text{Fe}^{3+}$ -cross-linked alginate hydrogels, encompassing from properties and synthesis to applications and future perspectives. We believe that this review would stimulate innovative ideas and promote the research of this material, leading to novel functional materials with new and emerging applications.

### 1. Introduction

Hydrogels are three-dimensional polymeric networks infiltrated with high amounts of water while maintaining their chemical structure.<sup>1</sup> Hydrogels undergo sol–gel transition as a response to chemical or physical stimuli and, by definition, must contain at least 10% of water in their gel state.<sup>2</sup> Their biocompatibility,<sup>3</sup>



**Ali Othman**

graduated with MSc in Chemistry from Jordan University of Science & Technology (Jordan) in 2008. Then, in 2019, he received PhD in Chemistry from Clarkson University (Potsdam, NY, USA). Presently, he is a Postdoctoral Research Associate at the Department of Chemistry & Biomolecular Science (Clarkson University). His research interests focus on development of novel functional nanomaterials and their applications for biosensing and environmental remediation, particularly using wearable bioelectronic devices. He co-authored over 20 peer-reviewed papers, 3 patents and 2 book chapters.



tunable biodegradability,<sup>4</sup> physiological stability<sup>5</sup> and structural and functional diversity<sup>6</sup> have situated hydrogels as the perfect candidates for biomedical applications<sup>7</sup> (e.g., drug delivery<sup>8</sup> and tissue engineering<sup>9</sup>). Recently, advances in hydrogel technologies have unlocked valuable capabilities for a wide range of various novel applications,<sup>10–12</sup> for example, in environmental science,<sup>13</sup> forensic science,<sup>14</sup> nanotechnology,<sup>15</sup> etc. Hydrogels can be produced from synthetic<sup>16</sup> or naturally occurring polymers (biopolymer).<sup>17</sup> Among the ever-increasing number of polymeric matrices that can undergo hydrogel formation, biomaterial-based hydrogels (e.g., alginate,<sup>18</sup> chitosan,<sup>19</sup> cellulose,<sup>20</sup> DNA,<sup>21</sup> polypeptides,<sup>22</sup> etc.) raised interest owing to their superior properties, particularly for bio-related applications.

Alginate is a polyanionic heteropolymer extracted from brown algae<sup>23</sup> or some genera of bacteria.<sup>24</sup> The biopolymer chain is composed of  $\beta$ -D-mannuronate (M) and  $\alpha$ -L-guluronate (G) linked through 1-4-glycosidic bonds (Fig. 1). These G and M moieties are arranged in polyguluronate (GG), polymannuronate (MM), and mixed GM domains distributed along the alginate chains. While alginic acid is not soluble in water, its salts, such as sodium or potassium alginates, can be dissolved forming viscous aqueous solutions. When an alginate aqueous solution finds certain divalent or trivalent cations, it undergoes instantaneous cross-linking forming ionotropic alginate hydrogels.<sup>25,26</sup> Ionotropic alginate hydrogels have been known and employed for decades for *in vivo* biomedical applications, environmental science, food science, and textile industry, among many other applications.<sup>18,27–34</sup>

The vast majority of applications and studies involving ionotropic alginate hydrogels employed  $\text{Ca}^{2+}$  as a cross-linking ion.

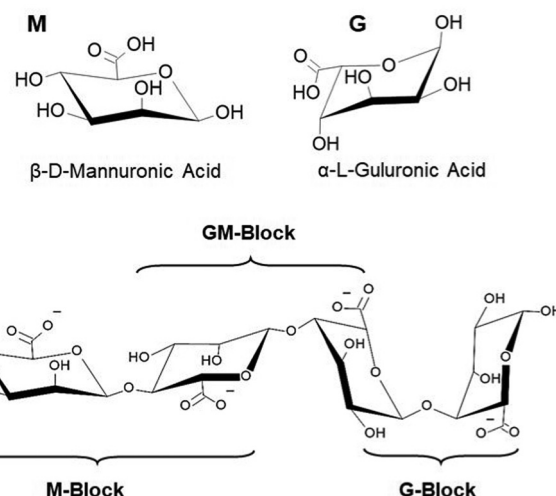


Fig. 1 Chemical structures of G and M alginate subunits and their arrangement in the biopolymer chain.

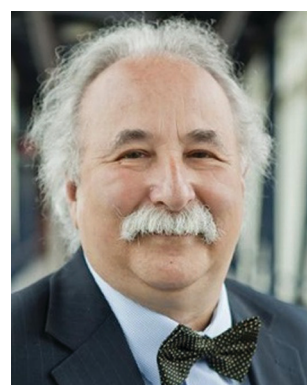
Calcium-cross-linked alginate hydrogels ( $\text{Ca}^{2+}$ -Alg) are well established and are commercially available, for example, as a cell culture matrix. The emphasis in research of  $\text{Ca}^{2+}$ -Alg has left behind other ionotropic hydrogels, such as  $\text{Fe}^{3+}$ -Alg or  $\text{Ba}^{2+}$ -Alg hydrogels. Nevertheless, in the last years, a dramatic increase in the publications involving  $\text{Fe}^{3+}$ -Alg hydrogels has been noticed. Two main reasons can explain this event, being the particular and exclusive chemistry of iron cations (e.g., coordination chemistry,<sup>35</sup> photochemistry<sup>36</sup>) the first. Second, the different cross-linking mechanism of trivalent cations to



Artem Melman

Artem Melman received his PhD in Organic Chemistry from the Weizmann Institute of Science (Rehovot, Israel) in 1997. He was a postdoctoral associate at the University of Oxford (1997–1999), a Lecturer at the Hebrew University of Jerusalem, and a Research Fellow at the National Institute of Diabetes, Digestive & Kidney Diseases (Bethesda, US). Since 2008 he was an Associate Professor at the Department of Chemistry & Biomolecular Science of Clarkson University.

University. He was an author of 75 papers in peer-reviewed international journals (Hirsch-index 24), 3 book chapters, and 11 patents. His research field was bioinorganic and medicinal chemistry, responsive biomaterials, and electrochemically controlled interfaces. Prof. Melman deceased in 2021 and is missed by friends and colleagues.



Evgeny Katz

Evgeny Katz received his PhD in Chemistry from Frumkin Institute of Electrochemistry (Moscow), Russian Academy of Sciences, in 1983. He was a senior researcher in the Institute of Photosynthesis (Pushchino, Moscow Region), Russian Academy of Sciences, in 1983–1991. In 1992–1993 he performed research at München Technische Universität (Germany) as a Humboldt fellow. Later, in 1993–2006, Dr Katz was a Research Associate Professor at the Hebrew University of Jerusalem. From 2006 he is Milton Kerker Chaired Professor at the Department of Chemistry & Biomolecular Science, Clarkson University (NY, USA). He has (co)authored over 500 papers in peer-reviewed journals/books with the total citation over 40 000 (Hirsch-index 93). His scientific interests are in the broad areas of bioelectronics, biosensors, biofuel cells and biocomputing. In 2019 he received international Katsumi Niki Prize for his contribution to bioelectrochemistry. In 2020 Katz was named Fellow of the International Society of Electrochemistry (ISE).



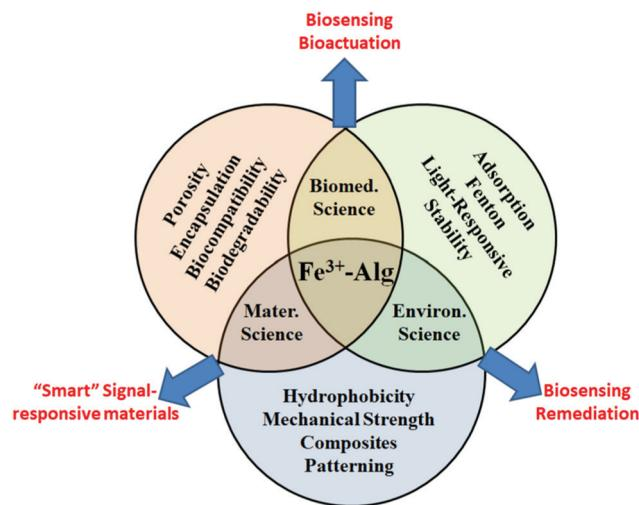


Fig. 2 Overview of the  $\text{Fe}^{3+}$ –Alg hydrogel properties and applications.

the alginate polymer has been found to provide novel features compared to those cross-linked by divalent ions. As a result,  $\text{Fe}^{3+}$ –Alg possess stimuli-responsiveness capabilities, redox properties, photosensitivity, enhanced mechanical stability, higher hydrophobicity, and higher absorptivity among other exceptional properties difficult to find in other ionotropic alginate hydrogels and other hydrogels in general. The versatility of the  $\text{Fe}^{3+}$ –Alg hydrogel has been acknowledged recently in the literature finding for it a wide range of applications, including drug delivery, tissue engineering or contaminant removal among others (Fig. 2).

The present review pretends to focus and describe, for the first time, all aspects of the research on  $\text{Fe}^{3+}$ –cross-linked alginate hydrogels ( $\text{Fe}^{3+}$ –Alg). This review paper is divided into two main sections. The first section is focused on  $\text{Fe}^{3+}$ –Alg physicochemical characteristics, synthesis and degradation strategies. The second section is dedicated to the state-of-the-art of current applications of this material. To conclude, challenges and perspectives are briefly analyzed.

## 2. Iron(III)-cross-linked alginate hydrogels – Preparation and Properties

### 2.1. Cross-linking mechanism

Alginic acid salts, such as sodium alginate ( $\text{NaAlg}$ ), are soluble in water forming viscous solutions. The biopolymer can undergo sol–gel transition in the presence of divalent (e.g.,  $\text{Ca}^{2+}$ ,  $\text{Ba}^{2+}$ ,  $\text{Pb}^{2+}$ ) or trivalent (e.g.,  $\text{Fe}^{3+}$ ,  $\text{Al}^{3+}$ ) cations forming ionotropic hydrogels.<sup>25,26,37–39</sup> The cross-linking by divalent cations can be explained by the so-called egg-box model in which two facing helical stretches of G sequences bind the divalent ion in a chelate type of binding.<sup>40–42</sup> The cross-linking mechanism and structure of trivalent cation complexes with alginate polymer remain under investigation.  $\text{Fe}^{3+}$  ion is a “hard” metal cation that tends to form complexes with ligands containing oxygen atoms, particularly in negatively charged

ligands such as carboxylate groups.  $\text{Fe}^{3+}$  complexes with polysaccharide ligands (e.g., chitosan,<sup>43</sup>  $\lambda$ -carrageenan<sup>44</sup> and alginate<sup>45</sup>) are very interesting because of their stability and unusual properties. On the other hand,  $\text{Fe}^{2+}$  ions have “soft” cationic features and bind preferably to neutral ligands containing nitrogen and sulfur atoms.  $\text{Fe}^{2+}$  ions poorly cross-link polysaccharides and do not convert alginate from its soluble state to a gel. The dramatic difference in the complex formation of  $\text{Fe}^{2+}$  and  $\text{Fe}^{3+}$  ions with carboxylate groups, particularly in alginate,<sup>46,47</sup> is evident from comparing stability constants of their citrate complexes which have  $\log K$  values 3.2 and 11.85, respectively.<sup>48</sup> Changing the oxidation state of iron cations can result in the reversible sol–gel conversion of alginate (Fig. 3). The limited information regarding the gelation process of  $\text{Fe}^{3+}$ –Alg arises from experimental complications associated with ferric ions, which produce insoluble hydroxides in water at neutral–basic pH values,<sup>49</sup> competing with the complex formation with alginate. Two gelation models have been proposed for the alginate cross-linking with  $\text{Fe}^{3+}$  ions. One model suggests that  $\text{Fe}^{3+}$  is coordinated by alginate resulting in spatially separated  $\text{Fe}^{3+}$  centers along with polysaccharides<sup>50,51</sup> and particularly in alginate hydrogel.<sup>45</sup> On the other hand, the colloidal model suggests that  $\text{Fe}^{3+}$  ions produce oxyhydroxide ( $\text{FeOOH}$ ) colloids stabilized by polysaccharide chains preventing aggregation of the colloidal species and keeping them in the hydrogel matrix.<sup>52</sup> Nevertheless, the literature found agreement in the following characteristics of  $\text{Fe}^{3+}$ –Alg cross-linking: (i)  $\text{Fe}^{3+}$  ions bind alginate stronger than most of other trivalent and divalent cations,<sup>53,54</sup> (ii)  $\text{Fe}^{3+}$  ions have a coordination number of 6 in the  $\text{Fe}^{3+}$ –Alg complex,<sup>55</sup> and (iii)  $\text{Fe}^{3+}$  has the capacity to bind not only with G blocks (as  $\text{Ca}^{2+}$  does) but also with MG blocks of alginate.<sup>56</sup> The different binding mechanism of  $\text{Fe}^{3+}$  ions compared to divalent ions such as  $\text{Ca}^{2+}$  has endowed  $\text{Fe}^{3+}$ –Alg with enhanced physicochemical properties as it will be discussed in the next section. The fraction of carboxylic groups that can bind the  $\text{Ca}^{2+}$  cation depends mostly on the amount of GG groups available for cross-linking. Thus, one could expect that the cross-linking of  $\text{Fe}^{3+}$ –Alg depends on the amount of GM and GG groups of the alginate polymer backbone which varies from one source to another. Chemical structures of  $\text{Fe}^{3+}$ –Alg can be found in the literature, but being far from certain and having merely a schematic character.<sup>57,58</sup> The coordination chemistry between  $\text{Fe}^{3+}$  cations and polysaccharides, including alginate, is still in the study and the outcomes of this research will be essential for a better understanding of  $\text{Fe}^{3+}$ –Alg synthesis, properties, and applications.

### 2.2. Physicochemical properties

The physicochemical properties of ionotropic alginate hydrogels made them very attractive for many applications.<sup>28–34,59</sup> In particular, biocompatibility and biodegradability have been exploited for tissue engineering<sup>60</sup> and regenerative medicine.<sup>61</sup> Regardless of the cross-linking ion, alginate hydrogels have physicochemical properties that are strongly dependent on the alginate source, concentration, and the gelation method.<sup>62,63</sup> However, given the different cross-linking mechanisms and the



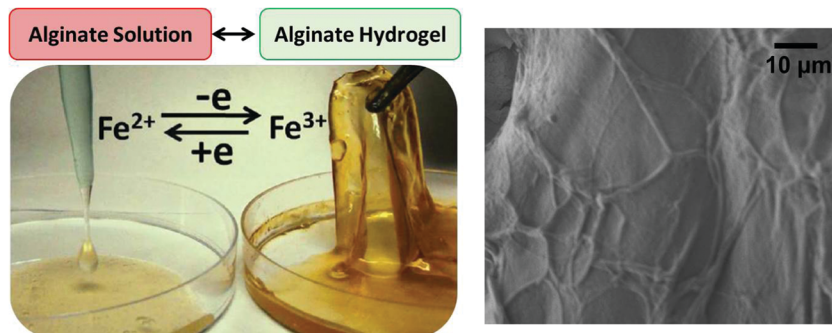


Fig. 3 Reversible sol–gel transition of alginate in the presence of  $\text{Fe}^{2+}$  and  $\text{Fe}^{3+}$  cations, respectively. Notably,  $\text{Fe}^{3+}$  cations effectively cross-link alginate resulting in the hydrogel formation, while  $\text{Fe}^{2+}$  cations are not capable of the hydrogel formation because of much weaker coupling to the alginate polymer. Redox transformation of  $\text{Fe}^{2+}/\text{Fe}^{3+}$  cations can change reversibly the alginate from its soluble state to the hydrogel and back (adapted from ref. 47. Copyright 2012 American Chemical Society). On the right, SEM image of the  $\text{Fe}^{3+}$ –Alg surface showing the characteristic brain-like morphology.

extraordinary chemistry of  $\text{Fe}^{3+}$  cations, certain physicochemical properties of  $\text{Fe}^{3+}$ –Alg have been found to be exceptional compared to other alginate hydrogels cross-linked with different metal cations (Table 1).

Upon introduction of gelling ions, the very rapid gel formation typically leads to heterogeneous structures characterized by wide pore size range and inhomogeneous cross-linking density, being higher in the external part than in the core of the gel. Visually,  $\text{Fe}^{3+}$ –Alg hydrogel has a yellowish to brown color (Fig. 3).<sup>47</sup> Under an electronic microscope,  $\text{Fe}^{3+}$ –Alg hydrogels display a rough surface with interconnected vessels resulting in a “brain-like” morphology (Fig. 3).<sup>64</sup> Because of the extended 3D-cross-linking with  $\text{Fe}^{3+}$  ions, a very wide pore size distribution with a large number of macro-pores is characteristic of the  $\text{Fe}^{3+}$ –Alg hydrogels (porosity ranging from a few nanometers to dozens of micrometers).<sup>65</sup> In the case of divalent cations, the egg-box model showed that divalent cations bind alginate in a planar two-dimensional (2D) manner resulting in less porous morphologies.<sup>66</sup> The different morphology and porosity of the iron cross-linked alginate hydrogel can explain the different swelling behavior of the  $\text{Fe}^{3+}$ –Alg compared to other ionotropic alginate gels. Alginate hydrogels are known to have fast swelling rates.<sup>67</sup> The increase in water content causes a decrease in cross-linking density, making the hydrogel softer and eventually triggering its fracture and dissolution. This might be a limiting factor for the hydrogel long-term use in biological fluids.<sup>68</sup> The  $\text{Fe}^{3+}$ –Alg hydrogels have shown slower swelling rates compared to their divalent analogue gels in both acidic and neutral environments.<sup>69,70</sup> This can be explained by the additional bonds

between chains that lead to the formation of a three-dimensional structure. The obtained higher density of crosslinks compared to that of divalent ions induces the decrease of the free volume and the water content. In addition, fast swelling rates are associated as well with the hydrophilicity of the hydrogel. A surface wettability study revealed that  $\text{Fe}^{3+}$ –Alg gels possess a less hydrophilic surface compared to that of divalent ion cross-linked gels since the contact angle measured for  $\text{Fe}^{3+}$ –Alg was approximately  $40^\circ$  while the one of  $\text{Ca}^{2+}$ –Alg was around  $10^\circ$ .<sup>71</sup>

Ionotropic alginate hydrogels are known to be relatively rigid but fragile. The capability of  $\text{Fe}^{3+}$  to bind both GG and GM groups of alginate results in a higher cross-linking density compared to that of  $\text{Ca}^{2+}$ –Alg. Hence a more compact network, endowed with better mechanical properties, such as deformability to compressive and extensional stresses or elastic modulus, can be obtained with  $\text{Fe}^{3+}$ –Alg hydrogels.<sup>69,70,72</sup>  $\text{Fe}^{3+}$ –Alg hydrogels were found to be 30–100% stiffer than  $\text{Ca}^{2+}$ –Alg given the higher cross-linking density with elastic modulus surpassing the 0.2 MPa. The  $\text{Fe}^{3+}$ –Alg hydrogels are all paramagnetic, meaning that the magnetization increases proportionally with increasing the applied magnetic field.<sup>72</sup> Alkali treatment of the hydrogel resulted in the formation of ferrous nanoparticles that provide the material with superparamagnetic properties.<sup>72,73</sup>

Overall, the binding  $\text{Fe}^{3+}$  to both GG and GM groups of the alginate polymer together with the higher binding affinity of  $\text{Fe}^{3+}$  with carboxylate-containing molecules has endowed the  $\text{Fe}^{3+}$ –Alg with superior physicochemical properties compared to  $\text{Ca}^{2+}$ –Alg. Since the major limitation of ionotropic alginate hydrogels is the leakage of cross-linking ions that weakens

Table 1  $\text{Ca}^{2+}$ –Alg vs.  $\text{Fe}^{3+}$ –Alg Properties

$\text{Ca}^{2+}$ –Alg	Properties	$\text{Fe}^{3+}$ –Alg
Binds GG groups	Alginate–ion interaction	Binds both GG and GM groups
Egg-box model	Binding structure	Unknown
Two-dimensional	Binding	Three-dimensional
Less	Porosity	More
Faster	Swelling rates	Slower
Softer and more flexible	Mechanical	Stiffer and more rigid
Highly hydrophilic	Surface	Less hydrophilic
None	Magnetic	Paramagnetic



the gel and eventually triggers its dissolution, the enhanced binding endows  $\text{Fe}^{3+}$ -Alg hydrogels with superior stability in particular in biofluids or solutions with high ionic strength. The slowest swelling rates and leakage of  $\text{Fe}^{3+}$  ions are an indirect confirmation of this superior stability which is indeed a huge improvement for the application of alginate hydrogels in long-term applications.

### 2.3. Hydrogel synthesis strategies

Several strategies have been developed for the synthesis of ionotropic alginate hydrogel films and particles. Methods for producing alginate hydrogels in macro- and nano-meter scales have been compiled in several reviews.<sup>74</sup> While these reviews are mainly focused on  $\text{Ca}^{2+}$ -Alg synthesis, most of the reported techniques can be extended to other cross-linking ions by replacing the gelling bath solution (typically containing  $\text{CaCl}_2$ ) for the one with the desired ion (e.g.,  $\text{FeCl}_3$ ). This section is meant to provide an introduction for the synthesis of  $\text{Fe}^{3+}$ -Alg based on the literature. These methods are expected to work regardless of the alginate composition. However, given the wide range of alginate sources, the optimized conditions reported should be revised and re-optimized for the specific alginate source and the final intended application.

For the majority of their applications, the  $\text{Fe}^{3+}$ -Alg hydrogels are used in the form of beads. The extrusion-dripping method is the most classic strategy for alginate bead synthesis due to its simplicity.  $\text{Fe}^{3+}$ -Alg beads can be synthesized by drop-wise addition of a NaAlg solution into a  $\text{Fe}^{3+}$ -containing solution. The beads are uniform in size and can be synthesized in a bulk quantity (Fig. 4A).<sup>75</sup> The formation and properties of  $\text{Fe}^{3+}$ -Alg beads produced from different iron salts have been reported.<sup>75</sup> The rapid diffusion of  $\text{Fe}^{3+}$  into the alginate droplet promotes the immediate bead formation resulting in a highly inhomogeneous hydrogel. Low amounts of  $\text{Fe}^{3+}$  can reach the inner core of the bead that remains soft and liquid, while the external part, with the high  $\text{Fe}^{3+}$  concentration, has a more rigid structure. The homogeneity of ionotropic alginate gels can be

controlled by different parameters.<sup>76</sup> Low molecular weight alginates and low concentration of a cross-linker ion lead to a highly inhomogeneous hydrogel. On the other hand, higher molecular weight alginates and larger concentrations of gelling ions lead to more homogenous ones. However, an alginate hydrogel formed from high molecular weight are usually undesirable due to their high viscosity. The same latter effect can be achieved if the gelation is done in the presence of non-gelling ions (e.g.,  $\text{Na}^+$ ).<sup>77</sup> Due to technique limitations, the minimum bead diameter that can be obtained with the drop-casting method is in the range of hundreds of micrometers. To achieve hydrogel particles with smaller diameters (micro- or nano-particles), water in oil emulsions<sup>78</sup> or microfluidic devices<sup>79</sup> can be employed.

Enzymatic reactions can be used to produce  $\text{Fe}^{3+}$ -Alg monodisperse nanoparticles.<sup>80</sup> Multi-copper oxidase enzyme laccase greatly accelerates the oxidation of  $\text{Fe}^{2+}$  to  $\text{Fe}^{3+}$  by dissolved oxygen. If the reaction is conducted in the presence of sodium alginate the reluctant  $\text{Fe}^{3+}$  cations are instantly trapped by alginate chains near the enzyme molecule producing a  $\text{Fe}^{3+}$ -cross-linked shell around it growing with nearly constant rates for every enzyme molecule. This process also depletes alginate chains from the solution, so, if the concentration of alginate is sufficiently low the reaction produces dispersion of highly homogeneous  $\text{Fe}^{3+}$  – alginate nanoparticles with their sizes tunable in the 30 to 300 nm range.

The redox properties of  $\text{Fe}^{2+}$  and  $\text{Fe}^{3+}$  cations can be exploited to electrodeposit  $\text{Fe}^{3+}$ -Alg onto an electrode surface. The electrodeposition of  $\text{Fe}^{3+}$ -Alg was reported first by our group.<sup>47,81</sup> Fig. 4B shows schematically the electrodeposition of an  $\text{Fe}^{3+}$ -Alg film onto an electrode immersed in a solution containing  $\text{Fe}^{2+}$ , NaAlg, and electrolyte (e.g.,  $\text{Na}_2\text{SO}_4$ ) needed for the electrochemical process, upon application of an oxidative potential. The oxidation of  $\text{Fe}^{2+}$  to  $\text{Fe}^{3+}$  at the electrode surface triggers the sol–gel transition of alginate, resulting in a thin  $\text{Fe}^{3+}$ -Alg layer. Note that the  $\text{Fe}^{2+}$  cations originally present in the solution do not cross-link alginate, while the electrochemically

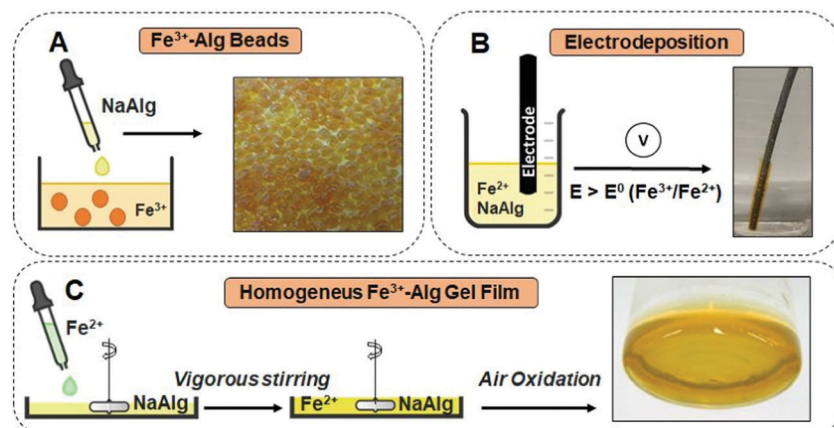


Fig. 4 Schematic representation of the preparation and visual appearance of: (A)  $\text{Fe}^{3+}$ -Alg beads (adapted from ref. 75. Copyright 2018 Elsevier). (B)  $\text{Fe}^{3+}$ -Alg electrodeposited film (adapted from ref. 127. Copyright 2020 American Chemical Society); (C) homogenous  $\text{Fe}^{3+}$ -Alg film (adapted from ref. 84 with permission). Abbreviation used in the figure: NaAlg – sodium alginate (soluble);  $\text{Fe}^{3+}$ Alg – iron(III)-cross-linked alginate (gel);  $E$  – potential applied on the electrode;  $E^0$  – redox potential of the  $\text{Fe}^{3+}/\text{Fe}^{2+}$  system.



generated  $\text{Fe}^{3+}$  cations do it. The electrodeposition conditions were optimized for a graphite electrode at 35 mM  $\text{Fe}^{2+}$ , 1.5% (w/v) NaAlg and 0.8 V (vs.  $\text{Ag}|\text{AgCl}$ ) for 60 seconds.<sup>47</sup> It should be noted that the required applied potential might be different for electrodes made of different materials or with chemically modified surfaces. The addition of the  $\text{Fe}^{2+}$ -containing solution (freshly prepared) into the alginate solution should be conducted under vigorous stirring to avoid the formation of  $\text{Fe}^{2+}$ -Alg clumps. The thickness of the layer depends mainly on the electrodeposition time.<sup>47</sup> The  $\text{Fe}^{3+}$ -Alg layer grows at the electrode surface upon continuing the electrodeposition process. However, with longer times the electron transfer becomes more difficult, obtaining less homogeneity and stability in the external region of the film. The  $\text{Fe}^{3+}$ -Alg film was characterized by cyclic voltammetry ( $E_{1/2} = 0.495$  V vs.  $\text{Ag}|\text{AgCl}$ ) showing a quasi-reversible redox process associated with the reduction/oxidation of iron cations.<sup>47,81</sup>

Highly homogenous alginate films can be accomplished by slowing down the gelation process. For example, the low solubility of  $\text{CaCO}_3$  has been employed for the synthesis of more homogenous  $\text{Ca}^{2+}$ -Alg gels.<sup>82,83</sup> As  $\text{CaCO}_3$  is getting solubilized at extremely low concentration,  $\text{Ca}^{2+}$  ions can slowly cross-link alginate resulting in uniform  $\text{Ca}^{2+}$ -Alg gels. Based on the same principle, using low concentrations of  $\text{Fe}^{3+}$  ions, homogenous  $\text{Fe}^{3+}$ -Alg films were synthesized.<sup>84,85</sup> Fig. 4C shows a schematic representation of the film synthesis. The slowly drop-wise addition of an  $\text{Fe}^{2+}$ -containing solution to a NaAlg solution under vigorous stirring produces a homogenous pale yellow solution. To prevent the formation of  $\text{Fe}^{2+}$ -Alg clumps an octagonal magnetic stirrer that allows instantaneous mixing was employed.<sup>84</sup> The gelation of alginate was limited by the slow oxidation of  $\text{Fe}^{2+}$  cations by the molecular oxygen present in the air resulting in a more homogenous hydrogel.<sup>85</sup> The hydrogel solidifies within 6 hours with 35 mM  $\text{Fe}^{2+}$  ion in the original solution, but it becomes slower if the concentration of  $\text{Fe}^{2+}$  is decreased.

Thin films of  $\text{Fe}^{3+}$ -Alg can be synthesized easily by the addition of NaAlg solution to an  $\text{Fe}^{3+}$ -containing solution. A commonly employed route for the synthesis of  $\text{Fe}^{3+}$ -Alg films is the solvent casting method.<sup>86</sup> Before the addition of the cross-linking solution, the water of the alginate solution is removed either by heating or freeze-drying.<sup>64,87</sup> The solvent cast process allows the synthesis of polymeric films without adulteration by heat or plasticizers.<sup>86</sup>

#### 2.4. Hydrogel dissolution/degradation

The presence of enough gelling cations (e.g.,  $\text{Ca}^{2+}$ ,  $\text{Fe}^{3+}$ ) guarantees the sol-gel transition forming an ionotropic alginate hydrogel. The hydrogel is stabilized by electrostatic interactions between the cations and the ionic components of alginate. This interaction is weaker than chemical bonds and hence it is expected that alginate hydrogels are susceptible to ion leakage and eventually, gel dissolution (gel-sol transition). This process is enhanced in the presence of cation chelating agents (e.g., citrate, EDTA, phosphate) and high concentrations of competing ions, such as  $\text{Na}^+$  or  $\text{K}^+$ .<sup>30,88</sup> Several attempts have been described in the literature to decrease gelling ion leakage

and to stabilize ionotropic alginate gels.<sup>89–92</sup> In addition, ionotropic alginate hydrogels can be degraded in the presence of lyase enzymes<sup>93–96</sup> or certain chemicals, such as sodium periodate.<sup>97</sup>

Ion leakage depends mainly on the binding strength with the alginate backbone. The leakage of  $\text{Ba}^{2+}$  cations was reported as minimal among other metal cations and the  $\text{Ba}^{2+}$ -Alg hydrogels are the most stable compared to other metal-alginate hydrogels.<sup>25,89</sup> The binding strength of  $\text{Fe}^{3+}$  to alginate was found to be similar to that of  $\text{Ba}^{2+}$ .<sup>98</sup> The leakage of  $\text{Fe}^{3+}$  cations from  $\text{Fe}^{3+}$ -Alg beads has been investigated in different conditions<sup>55,69</sup> being influenced by the surrounding conditions such as ionic strength, pH and temperature. Within 24 hours, 30% of the  $\text{Fe}^{3+}$  leaked from the  $\text{Fe}^{3+}$ -Alg beads in HCl (pH 1.2), while 15% leaked in PBS (pH 7.4).<sup>55</sup> Similar results were reported by other research groups.<sup>69</sup> At low pH, carboxylate groups of the polysaccharide get protonated,<sup>99</sup> and the electrostatic interaction with  $\text{Fe}^{3+}$  is no longer effective. Thus, faster diffusion of  $\text{Fe}^{3+}$  from the  $\text{Fe}^{3+}$ -Alg gels can be expected.

As it will be described in more details later (see Section 3.2), leakage of  $\text{Fe}^{3+}$  cations and eventual dissolution of the  $\text{Fe}^{3+}$ -Alg hydrogels do not allow their long term applications (e.g., in scaffolds), in which superior hydrogel stability is required. However, for some other applications hydrogel instability will be beneficial (e.g., for drug delivery; Sections 3.1–3.3). In this section the main strategies for  $\text{Fe}^{3+}$ -Alg hydrogel dissolution are presented. The optimized conditions reported may differ depending on the alginate source.

The electrodeposition of  $\text{Fe}^{3+}$ -Alg onto an electrode surface added an additional feature to the ionotropic alginate hydrogels.<sup>47</sup> The electro-responsive hydrogel can be de-gelled upon application of a reductive potential converting the cross-linking  $\text{Fe}^{3+}$  cations back to  $\text{Fe}^{2+}$  cations which cannot keep alginate at the electrode surface, thus resulting in the hydrogel dissolution and removal from the electrode surface. As Fig. 5A shows, the alginate film gets dissolved, stimulated by the electric potential, when the  $\text{Fe}^{3+}$  cations are reduced to  $\text{Fe}^{2+}$  cations.<sup>100</sup> The effect of the reductive potential value on the rate of the  $\text{Fe}^{3+}$ -Alg layer dissolution was studied and the applied potential was optimized for different layer thicknesses.<sup>47</sup> The applied potential of 0.1 V (vs.  $\text{Ag}|\text{AgCl}$ ) was enough to reduce partially  $\text{Fe}^{3+}$  to  $\text{Fe}^{2+}$ , in 30 minutes, but in the same time frame, -1.0 V was enough to reduce all  $\text{Fe}^{3+}$  cations and dissolve the  $\text{Fe}^{3+}$ -Alg layer completely. The slow charge propagation across the polymer film may inhibit the electro-dissolution. The higher reductive potential applied provides a larger driving force for the redox process facilitating the de-gelation process. The charge propagation gets even more difficult when the  $\text{Fe}^{3+}$ -Alg layer is thicker. The electro-responsive feature is inherent of  $\text{Fe}^{3+}$ -Alg and cannot be found in other ionotropic hydrogels, while some other mechanisms for the electro-response of hydrogels have been reported.<sup>101</sup>

$\text{Fe}^{3+}$ -Chelating agents, such as phosphate and citrate ions, bind  $\text{Fe}^{3+}$  ions stronger than alginate, thus, facilitating the  $\text{Fe}^{3+}$  ions leakage from the  $\text{Fe}^{3+}$ -Alg hydrogel. This process is accompanied by the diffusion of sodium ions ( $\text{Na}^+$ ) and water

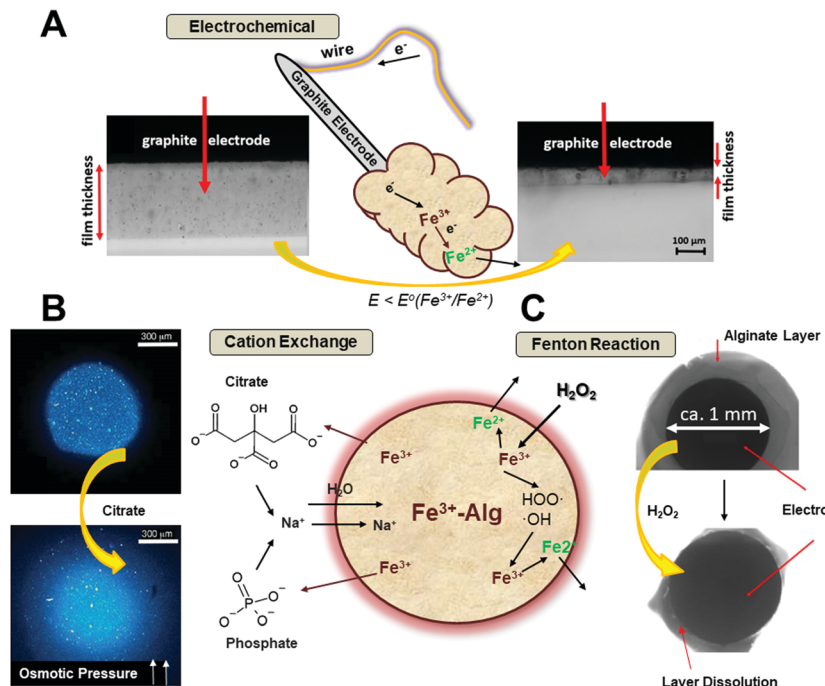


**Fig. 5** Schematic representation of the  $Fe^{3+}$ –Alg de-gelation mechanism and visual appearance stimulated by: (A) electric potential (adapted from ref. 100. Copyright 2017 Wiley-VCH); (B) chelating ions (adapted from ref. 103. Copyright 2012 Royal Society of Chemistry); (C) hydrogen peroxide (adapted from ref. 106. Copyright 2017 Wiley-VCH).

into the hydrogel (Fig. 5B), increasing the osmotic pressure inside the gel.<sup>102</sup> Therefore, the gel swells increasing its size and eventually, when not enough cross-linking ions are present, the gel will collapse (Fig. 5B).<sup>103</sup> The de-gelation kinetics leading to the hydrogel degradation and dissolution depends on the chelating ion concentration, being faster when the concentrations are higher. Physiological concentrations of ascorbic acid and citrate have been employed to study the de-gelation process of  $Fe^{3+}$ –Alg beads.<sup>103</sup>

Another  $Fe^{3+}$ –Alg hydrogel degradation process can proceed in the presence of  $H_2O_2$ , as shown in Fig. 5C schematically. The reaction cascade leading to the alginate hydrogel degradation is based on a Fenton-type reaction<sup>104</sup> (the “•” symbol denotes an unpaired electron):



These reactions, catalyzed either by iron cations present in the hydrogel or added externally,<sup>105</sup> produce reactive oxygen species (free radicals  $HO^\bullet$ ), which react with guluronate and/or manuronate subunits of alginate chains, resulting in alginate chain degradation and the hydrogel dissolution.<sup>106</sup> This reaction produces free alpha-oxy radicals that reduce  $Fe^{3+}$  cations back into  $Fe^{2+}$  state which regenerate new radicals, thus continuing the radical chain reaction. The dissolution of  $Fe^{3+}$ –Alg by  $H_2O_2$  added a new feature in the wide use of alginate as a signal-responsive material. Hydrogen peroxide can be produced *in situ* in course of many enzymatic reactions (typically catalyzed by oxidases, *e.g.*, glucose oxidase, lactate oxidase, *etc.*) activated by various biomolecule substrates (*e.g.*, glucose, lactate, *etc.*). It should be noted that  $H_2O_2$  is present in biofluids (blood, urine, *etc.*)<sup>107</sup> at small concentrations (1–5  $\mu$ M) under normal

physiological conditions<sup>108</sup> or at elevated concentrations under pathophysiological conditions,<sup>109</sup> both sufficient for oxidative decomposition of  $Fe^{3+}$ –Alg, thus allowing its use as a drug-delivering matrix with the drug release stimulated by  $H_2O_2$ .

Finally, yet importantly, light induced dissolution of  $Fe^{3+}$ –Alg has been achieved in presence of sacrificial carboxylates.<sup>85,110</sup> The well-known photoreduction of  $Fe^{3+}$  to  $Fe^{2+}$  in iron carboxylate complexes<sup>36,111,112</sup> can be exploited for dissolution of the  $Fe^{3+}$ –Alg hydrogels. The photo-responsive behavior of  $Fe^{3+}$ –Alg hydrogels with different carboxylates has been studied, concluding that compounds containing an  $\alpha$ -hydroxyl carboxylic group (*e.g.*, lactic acid) had higher photoreduction rates than those without  $\alpha$ -hydroxyl carboxylic group (*e.g.*, butyric acid).<sup>85</sup>

### 3. Iron(III)-cross-linked alginate hydrogels – applications

The above overviewed physicochemical properties of the  $Fe^{3+}$ –Alg hydrogels have been exploited in the last decade for a broad range of applications. The rich chemistry of  $Fe^{3+}$ –Alg hydrogels allowed applications which are not possible for other hydrogels, particularly not achievable with the broadly used  $Ca^{2+}$ –alginates. The wide versatility of  $Fe^{3+}$ –Alg hydrogels is gathered and analyzed in this section.

#### 3.1. Drug delivery

An enormous amount of polymeric matrices has been developed and used for drug delivery applications.<sup>113,114</sup> These materials enhanced therapeutic treatments by (i) allowing targeted delivery



of the drug; (ii) protecting the drug from degradation, and (iii) preventing undesired immunologic response. Alginate hydrogels (mostly exemplified by  $\text{Ca}^{2+}$ -alginates) have been implemented for delivery systems because of their biocompatibility, ease of synthesis, and high encapsulation efficiency.<sup>115</sup> Ionotropic alginate hydrogels have been employed for encapsulation and release of nanoparticles,<sup>116</sup> proteins,<sup>117</sup> enzymes,<sup>118</sup> growth factors,<sup>119</sup> small molecules,<sup>117</sup> and DNA<sup>120</sup> among many other bioactive species.<sup>121</sup>

The delivery processes of most alginate systems are based on diffusion out of encapsulated species through the alginate pores. Small molecules diffuse faster than larger ones and negatively charged molecules diffuse out of the negatively charged alginate matrix faster than the positively charged ones. The kinetics of the release, so-called conventional release or leakage (Fig. 6), is highly influenced by the surrounding conditions (pH and temperature) and the physicochemical properties of the entrapped (bio)molecules (size, concentration, and isoelectric point). The release time-profile is characterized by an initial burst release that slows down as the gel empties. The uncontrolled release (leakage) of the loaded species is typical for  $\text{Ca}^{2+}$ -cross-linked alginate hydrogels.<sup>122</sup> The leakage process is obviously controlled by the system composition and its environment, but it is not triggered by any specific signal.

“Smart” drug delivery systems permit a more controllable drug release and have multiple advantages compared to the conventional release (leakage) (Table 2). These materials can encapsulate drug payload and release it at specific targets (targeted delivery) or in specific environments (signal-triggered delivery). The several possibilities to dissolve the  $\text{Fe}^{3+}$ -Alg hydrogel (Section 2.4) make it a multi stimuli-responsive material (light, pH, electric,  $\text{H}_2\text{O}_2$ ) with promising applications for signal-triggered and “smart” release of (bio)molecules or drugs.<sup>123</sup> This responsiveness, a key characteristic of the  $\text{Fe}^{3+}$ -Alg, cannot be found in other ionotropic alginate hydrogels (cross-linked with other metal cations  $\text{Ca}^{2+}$ ,  $\text{Ba}^{2+}$ , etc.) since it is particular of  $\text{Fe}^{3+}$  ions. The unique properties of the  $\text{Fe}^{3+}$  cross-linking cations are mostly based on their redox transformation to  $\text{Fe}^{2+}$  cations, which do not keep alginate in the gel state. When the signal is present in the surroundings of the system, the  $\text{Fe}^{3+}$ -Alg gets dissolved producing

Table 2 Advantages of “Smart” (signal-triggered) vs. Conventional Release (leakage)

Conventional release (leakage)	“Smart” (signal-triggered) release
Uncontrolled release profile	Defined drug release profile
Poor drug adsorption	Specific targeting
Premature metabolism/degradation	Drug protection
Side effects	Better patient compliance
Poor drug bioavailability	Enhanced bioavailability

a burst release of entrapped (bio)molecules or drugs (Fig. 6). The release is no longer only dependent on the properties of the payload and a similar time-dependent release profile can be expected for any encapsulated molecule in the hydrogel.

### 3.2. Conventional release (leakage)

Delivery of small molecules (e.g., ibuprofen,<sup>66</sup> folic acid<sup>124</sup>) or proteins, (e.g., BSA frequently used as a model protein<sup>69</sup>) from millimeter-sized  $\text{Fe}^{3+}$ -Alg beads has been analyzed under different conditions. The  $\text{pK}_a$  of alginic acid is situated around 3.5. The guluronic and mannuronic acid moieties of alginate become protonated at acidic pH < 3.5 and the resultant hydrogel is no longer supported by electrostatic interactions, but by hydrogen bonding only (Fig. 7A).<sup>125</sup> As a result, the hydrogel shrinks leading to a less porous material. For example, the release profile of ibuprofen (Fig. 7B) is very fast (a few hours of time-scale) under neutral pH conditions.<sup>66</sup> This can be explained by the high porosity of  $\text{Fe}^{3+}$ -Alg hydrogels. However, the release of small molecules was significantly delayed at acidic pH values due to the above-mentioned reason. The same phenomenon was observed for the delivery of proteins, such as BSA (Mw. 66 kDa). However, in this instance, the release of proteins was delayed much more (up to 30 h) due to the larger size of BSA molecules (Fig. 7C).<sup>69</sup> The conventional release of molecules was highly influenced by the presence of chelating agents such as phosphate ( $\text{PO}_4^{3-}$ ). Then, the erosion of  $\text{Fe}^{3+}$ -Alg enhanced remarkably the release rates of proteins and small molecules (Fig. 7B and C).<sup>66,69</sup> In a similar approach, significant increase in the release rates of small molecules of rhodamine 6G was observed in the presence of citrate ions

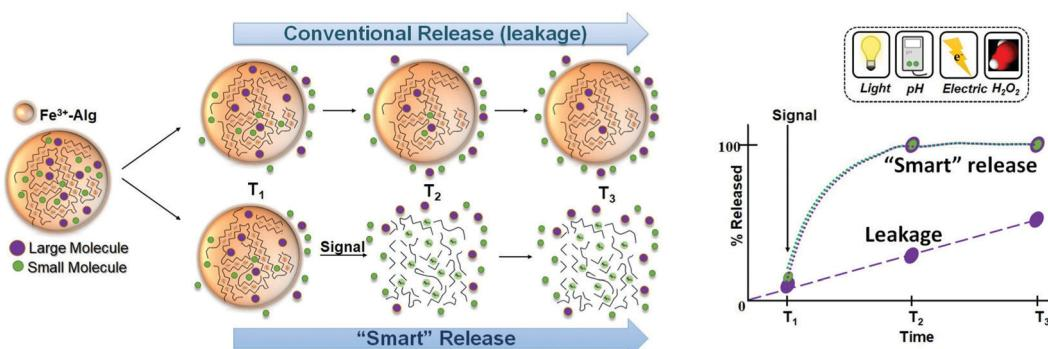


Fig. 6 Schematic representation of conventional release (leakage) and “Smart” signal-triggered release of molecules from  $\text{Fe}^{3+}$ -Alg hydrogel and their time-dependent release profiles.



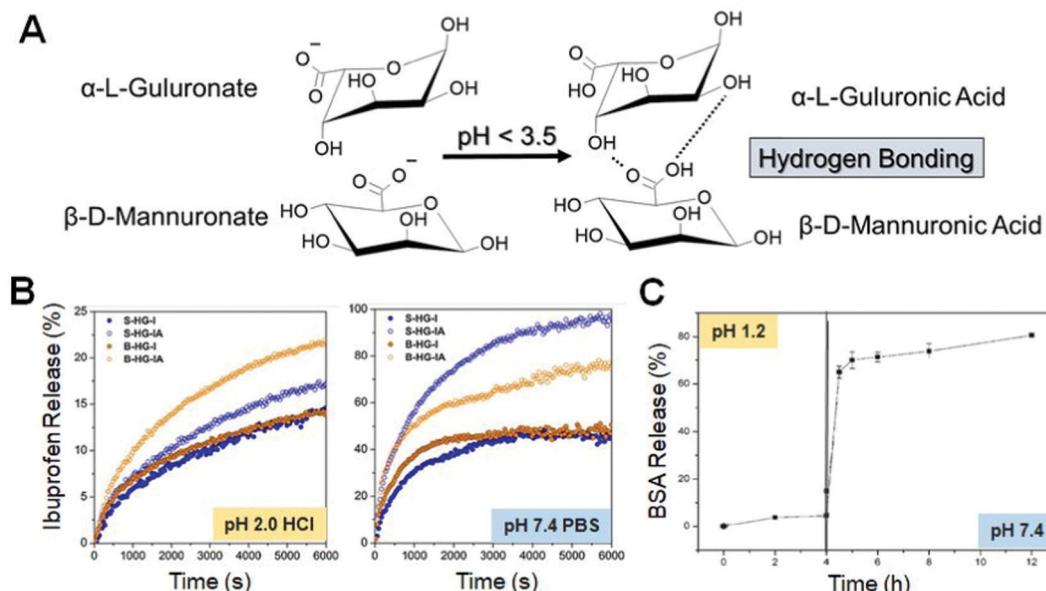


Fig. 7 (A) Alginate monomers chemical structures below and above the alginate  $pK_a$  value. (B) Release of ibuprofen at pH 2.0 and pH 7.4; the curves correspond to differently prepared samples – see the original publication for details (adapted from ref. 66. Copyright 2018 Elsevier). (C) BSA release in different pH solutions (adapted from ref. 69. Copyright 2015 Wiley-VCH).

(note that citrate binds  $\text{Fe}^{3+}$  ions stronger than phosphate ions).<sup>103</sup> The conventional release (leakage) of DNA from  $\text{Fe}^{3+}$ -Alg films electrodeposited on an electrode surface has been experimentally analyzed and modeled theoretically.<sup>126–128</sup> The release kinetics of DNA was extremely fast due to the presence of negatively charged phosphate groups in DNA resulting in great repulsion within the negatively charged alginate matrix.<sup>127</sup>

### 3.3. “Smart” (signal-triggered) release

In this section, the signal-triggered release of (bio)molecules (“smart” delivery) from  $\text{Fe}^{3+}$ -Alg is discussed and analyzed.

**3.3.1. Electrochemically stimulated release.** The electrodeposition and electro-stimulated dissolution of  $\text{Fe}^{3+}$ -Alg hydrogels on an electrode surface have been reported recently.<sup>47</sup> The electrochemical deposition of the  $\text{Fe}^{3+}$ -Alg film onto a graphite electrode was performed from an aqueous solution containing alginate and  $\text{Fe}^{2+}$  cations upon application of +0.8 V (vs.  $\text{Ag}|\text{AgCl}$ ). Electrochemical oxidation of the  $\text{Fe}^{2+}$  cations resulted in the production of  $\text{Fe}^{3+}$  cations near the electrode surface, then rapidly cross-linking the alginate and forming a hydrogel film growing at the electrode surface. When BSA was added to the solution, it was physically entrapped into the growing alginate film. The amount of the entrapped protein was dependent on its concentration in the parent solution and the thickness of the alginate hydrogel film deposited on the electrode surface. Changing the electrode potential to the reductive values (+0.1, -0.4 or -1.0 V vs.  $\text{Ag}|\text{AgCl}$ ; all thermodynamically sufficient for the  $\text{Fe}^{3+}$  reduction) resulted in returning iron cations inside the film to  $\text{Fe}^{2+}$  cations, which are not capable to cross-link the alginate polymer, then dissolving the hydrogel film and releasing the loaded BSA. The rate of the alginate dissolution and the BSA release process was dependent

on the potential applied and it was increased with the reductive potential elevated. Under optimized conditions, the vast majority of BSA was released in less than 30 minutes.<sup>47</sup> Notably, the electrochemically stimulated release was much faster than the BSA leakage from the alginate film. While the first study included the BSA load and then electrochemically stimulated release, considering BSA as a convenient model, real drugs and other bioactive substances can be released from the  $\text{Fe}^{3+}$ -Alg-modified electrodes in a similar way. In a similar approach, entrapped lysozyme (an antimicrobial enzyme) was electrochemically released and then applied to an agar plate swabbed with *Micrococcus luteus* (a Gram-positive bacteria) resulting in inhibition of the bacteria growth.<sup>81</sup> It should be noted that the electrical potentials and  $\text{Fe}^{3+}$  reductive current were applied on the  $\text{Fe}^{3+}$ -Alg-modified electrodes using an external electric device (an electrochemical analyzer).

In a more interesting approach the electrochemical release system can operate as a self-powered device in a way similar to biofuel cells.<sup>129,130</sup> The  $\text{Fe}^{3+}$ -Alg-modified electrode containing pre-loaded biomolecules or drugs operated as a cathode producing current for the  $\text{Fe}^{3+}$  reduction stimulating the alginate dissolution and the payload release. Its operation was not different from that described above. However, the difference was in the operation of the anode electrically coupled to the releasing electrode. The anode produced the reductive potential and current for the operation of the releasing electrode and the system did not require any external source of electric power for stimulating the release process. In other words, the whole device was self-powered similarly to a biofuel cell. In the first system, the reductive potential was generated at the anode using NADH as electron-donating species (Fig. 8A). NADH was produced enzymatically in various ways, mimicking Boolean logic operations,<sup>131</sup> through reactions catalyzed by different enzymes (Fig. 8B), and then it was electrocatalytically oxidized to



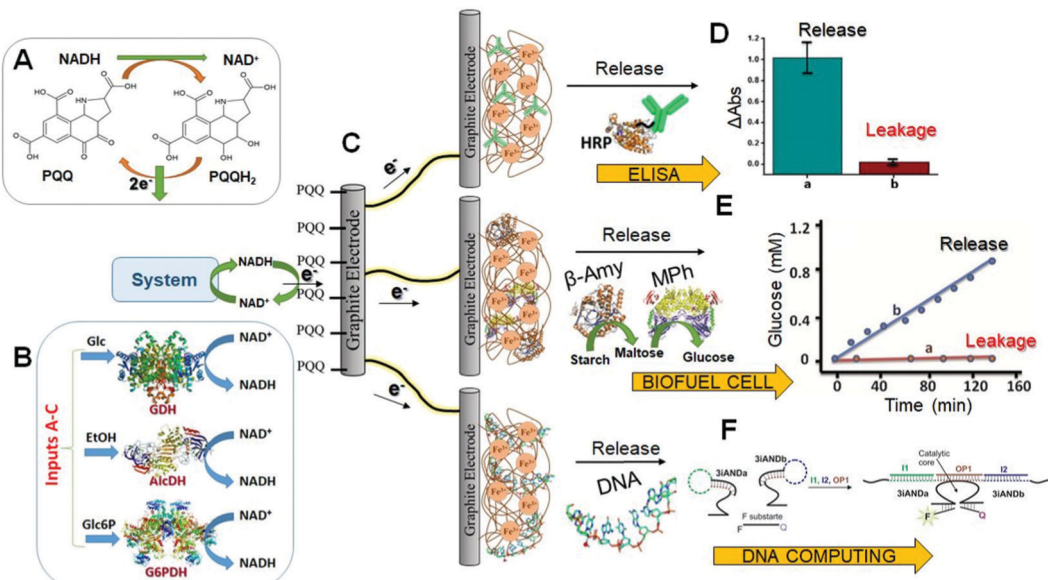


**Fig. 8** (A) NADH oxidation catalyzed in the presence of PQQ. (B) Enzyme-catalyzed NADH production; three different enzymes were activated with three substrates operating in parallel. (C) Schematic representation of a typical  $\text{Fe}^{3+}$ -Alg electrode used for: (D) release of antibodies (adapted from ref. 103. Copyright 2014 Royal Society of Chemistry); (E) release of enzymes, then producing glucose from starch for biofuel cell operation (adapted from ref. 134. Copyright 2014 Wiley-VCH); and (F) release of DNA, then activating a DNAzyme for DNA computing operation (adapted from ref. 135. Copyright 2015 Wiley-VCH). Abbreviations used in the figure: GDH – glucose dehydrogenase; AlcDH – alcohol dehydrogenase; G6PDH – glucose 6-phosphate dehydrogenase; Glc – glucose; EtOH – ethanol; Glc6P – glucose-6-phosphate; HRP – horseradish peroxidase;  $\beta$ -Amy –  $\beta$ -amylase; MPH – maltose phosphorylase.

form  $\text{NAD}^+$  at a pyrroloquinoline quinone (PQQ)-modified electrode (Fig. 8C). It should be noted that PQQ is an efficient electrocatalyst for oxidation of NADH, particularly in the presence of  $\text{Ca}^{2+}$  cations in solution.<sup>132</sup> The reductive potential generated biocatalytically at the anode was transferred to the  $\text{Fe}^{3+}$ -Alg releasing electrode (cathode) connected to the anode with a conducting wire. This system was employed for: (a) the release of an antibody complex (Fig. 8D) that reacted with a complementary-target mimicking a targeted delivery biomedical process;<sup>133</sup> (b) the release of  $\beta$ -amylase ( $\beta$ -Amy) and maltose phosphorylase (MPH) (Fig. 8E) that were biocatalytically degrading starch to yield glucose that was further employed in a biofuel cell;<sup>134</sup> (c) release of a DNA strand that can hybridize with the complementary strand activating a deoxyribozyme (DNAzyme)<sup>135</sup> utilized in a DNA computing system<sup>136</sup> (Fig. 8F). In another configuration, a biocatalytic anode was activated for producing the reductive potential/current in the presence of bacterial cells (*E. coli*)<sup>137</sup> or antibodies,<sup>138</sup> then stimulating release processes at the connected  $\text{Fe}^{3+}$ -Alg electrode. The process stimulated in the presence of *E. coli* cells resulted in the Polymyxin B (antibacterial drug) release, then inhibiting the bacteria proliferation.<sup>137</sup> Importantly, this system realized negative feedback when the bacteria appearance resulted in the bacteria growth inhibition.

The biocatalytic anode used for stimulation of the releasing  $\text{Fe}^{3+}$ -Alg electrode can be activated by different means, using well-established processes typical for various biosensors and biofuel cells.<sup>139</sup> In one of the possible configurations, the biocatalytic anode was functionalized with PQQ-dependent glucose dehydrogenase (PQQ-GDH) oxidizing glucose (Glc) to gluconic acid (GlcA) and producing the reductive potential/

current utilized at the connected  $\text{Fe}^{3+}$ -Alg electrode to release the entrapped Protein A.<sup>140</sup> While glucose present in the solution was used as the electron donor for the anodic process, the anode activation or inhibition (ON/OFF switch) was achieved by pH changes produced *in situ* by other enzymes mimicking Boolean Not-XOR logic operation. Finally, the release of Protein A from the alginate-electrode was stimulated when the PQQ-GDH-modified anode was in the ON-state controlled through the logic operation. The present system illustrated the possibility of the release function controlled by orthogonal biocatalytic processes switching ON-OFF the biocatalytic reaction at the connected anode. Various biomolecule association/dissociation processes proceeding at the biosensing anode and controlled by pH changes<sup>141</sup> or biomolecule signals<sup>142</sup> were utilized to activate the biocatalytic anode and then to trigger the release process from the connected  $\text{Fe}^{3+}$ -Alg-modified electrode. The versatility of the biochemical reactions used for activation of the release process allows construction of various systems for numerous applications. Some of them provide background for future biomedical applications. For example, a system releasing insulin in response to the ketone body (a biomarker of ketoacidosis) was tested *in vitro*,<sup>142</sup> but its *in vivo* operation is potentially possible, at least conceptually.

**3.3.2. Release stimulated by  $\text{H}_2\text{O}_2$ .** Alginate hydrogel can be disrupted by oxygen-containing free radicals ( $\cdot\text{OH}$  and  $\cdot\text{OOH}$ ) produced through a Fenton-type reaction of  $\text{H}_2\text{O}_2$  catalyzed by iron cations ( $\text{Fe}^{3+}/\text{Fe}^{2+}$ ) (see Section 2.4). Then, biomolecule/bioactive species loaded in the  $\text{Fe}^{3+}$ -Alg matrix (e.g., DNA<sup>106,127</sup> or insulin<sup>143</sup>) are released upon alginate decomposition. The  $\text{H}_2\text{O}_2$  can be directly added to a solution,

then defusing into the  $\text{Fe}^{3+}$ -Alg hydrogel resulting in its decomposition and the entrapped species release.<sup>127</sup> In this case,  $\text{H}_2\text{O}_2$  is a primary chemical signal activating the release process. Alternatively,  $\text{H}_2\text{O}_2$  can be produced *in situ* in reactions catalyzed by enzymes (oxidases)<sup>106,143,144</sup> or by nanozymes (inorganic nanoparticles mimicking enzyme reactions).<sup>127</sup> Then, the catalytic reactions leading to  $\text{H}_2\text{O}_2$  production are activated by enzyme substrates serving as primary signals. The reactions can be catalyzed by a single enzyme or nanozyme activated by one substrate (e.g., glucose oxidase, GOx, activated with glucose<sup>143</sup> or Au-NP nanozyme also activated with glucose<sup>127</sup>) or by several enzymes catalyzing a reaction cascade in the presence of various substrates operating as primary input signals.<sup>106,144</sup> The complex biocatalytic cascades activated by different combinations of the substrate-inputs can mimic various Boolean logic gates.<sup>145</sup> Importantly, glucose serving as a primary input signal can stimulate insulin release, thus, realizing a physiologically meaningful combination of the input signal (glucose) and output result (insulin release).<sup>143</sup>

The reactions producing  $\text{H}_2\text{O}_2$  can be catalyzed by enzymes bound to the alginate interface, then the generated  $\text{H}_2\text{O}_2$  diffuses into the alginate hydrogel and partially escapes to the solution.<sup>106</sup> The  $\text{H}_2\text{O}_2$  fraction that penetrates into the hydrogel is catalytically decomposed to yield free radicals, which disrupt the alginate polymeric chains leading to the release of the loaded species (Fig. 9A). In another configuration, the enzymes or nanozymes can be included in the alginate matrix and produce  $\text{H}_2\text{O}_2$  internally in the hydrogel resulting in its dissolution and then payload release. The nanozymes<sup>146,147</sup> (catalytic nanoparticles) are large enough for not leaking out prior to the reaction producing  $\text{H}_2\text{O}_2$ . While nanozymes are less specific to a substrate comparing with enzymes, they are more stable providing longer storage and operational time. The enzymes are much smaller and can leak out from the hydrogel prior to its dissolution. In order to keep them inside the hydrogel, the enzymes can be bound to nanoparticles (e.g.,  $\text{SiO}_2$ -NPs; 200 nm diameter) increasing effectively the size of the catalytic species and reducing their leakage (Fig. 9B).

**3.3.3. Release stimulated by light.** The photoreduction of  $\text{Fe}^{3+}$  ions to  $\text{Fe}^{2+}$  in the presence of  $\alpha$ -carboxylic acids operating

as sacrificial electron donors has been employed to design light-responsive  $\text{Fe}^{3+}$ -Alg hydrogels.<sup>85</sup> The photochemical reduction of  $\text{Fe}^{3+}$  resulted in removal of the cross-linking cations (note that the produced  $\text{Fe}^{2+}$  cations do not cross-link the alginate chains) and dissolution of the hydrogel accompanied by the release of species entrapped in the hydrogel. The combination of lactate and the  $\text{Fe}^{3+}$ -Alg hydrogel prepared in the form of nano-size species was successfully implemented for photo-triggered release of folic acid.<sup>110</sup> Similarly,  $\text{Fe}^{3+}$ -Alg films interpenetrated with cellulose were used as photo-responsive matrices for delivery of small molecules of dexamethasone (a corticosteroid drug) and larger BSA protein molecules.<sup>148</sup> While small drug molecules entrapped in the  $\text{Fe}^{3+}$ -Alg hydrogel were leaking fast, the irradiation of the hydrogel with visible light significantly facilitated their release process. The difference between the leakage and light-induced release was even greater for the larger protein molecules, which demonstrated much smaller leakage prior to the irradiation and the fast release after it.<sup>148</sup> Surprisingly,  $\text{Fe}^{3+}$ -Alg hydrogel beads were able to release small molecules (folic acid and Congo Red dye) upon light irradiation in the absence of the sacrificial  $\alpha$ -carboxylic acid electron donor.<sup>149</sup> It should be noted that the photophysical and photochemical mechanisms of the light-triggered decomposition of the  $\text{Fe}^{3+}$ -Alg hydrogel leading to the release processes are not fully understood and require additional studies.

### 3.4. Biomedicine: from *in vitro* to *in vivo* applications

Alginate hydrogels as matrices for 2D and 3D cell cultures have been extensively used owing to their biocompatibility and low cytotoxicity.<sup>150</sup> *In vitro* cell culture studies are essential to make a costless drug development process, increase therapeutic efficacy and understanding drug mechanisms of action. In addition, cell growth in alginate hydrogels are of great relevance for tissue engineering and regenerative medicine applications.<sup>61</sup> Alginate hydrogels have been extensively used for cell culture studies due to their high water content, porosity (diffusion of nutrients in and waste out) and optical transparency important for microscope analysis. Cell culture matrix kits based on alginate hydrogels are commercially available confirming their feasible present and future applications in this field.

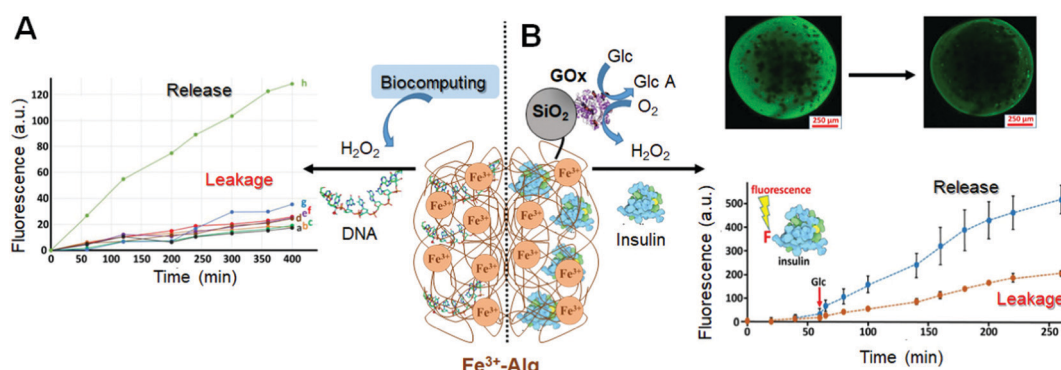


Fig. 9 (A) DNA release from the  $\text{Fe}^{3+}$ -Alg hydrogel triggered by  $\text{H}_2\text{O}_2$  produced through biocatalytic reactions (Adapted from ref. 106. Copyright 2017 Wiley-VCH). (B) Insulin release from the  $\text{Fe}^{3+}$ -Alg hydrogel triggered by glucose (adapted from ref. 143. Copyright 2017 Wiley-VCH). Abbreviations used in the figure: GOx – glucose oxidase; Glc – glucose; Glc A – gluconic acid (glucose oxidation product).



Despite the fact that the vast majority of the cell culture studies have been performed on  $\text{Ca}^{2+}$ -cross-linked alginate hydrogels, there is a growing interest in the use of the  $\text{Fe}^{3+}$ -Alg hydrogels as matrices for the 2D and 3D cell cultures in the last few years. In a pioneer study, the effect of the alginate biopolymer composition on the growth of human dermal fibroblasts (HDF) was studied.<sup>151</sup> It was found that the  $\text{Fe}^{3+}$ -Alg hydrogels with the high content of G and M subunits have similar efficacy for promoting cell proliferation (Fig. 10A and B). However, the  $\text{Fe}^{3+}$ -Alg hydrogel with the high M content required additional stabilization in cell culture media for 8 days.<sup>151</sup> Then, the *in vitro* cell adhesion was analyzed for the alginate hydrogels cross-linked with  $\text{Fe}^{3+}$  and  $\text{Ca}^{2+}$  cations. While the  $\text{Fe}^{3+}$ -Alg hydrogel demonstrated good proliferation of cells, the  $\text{Ca}^{2+}$ -cross-linked alginate hydrogel did not.<sup>152</sup> Vitronectin, a glycoprotein responsible for cell adhesion, migration, and proliferation on different culture media,<sup>153</sup> plays an important role in cell culturing on alginate hydrogels. Therefore, the adsorption of vitronectin on alginate hydrogels of different compositions was studied. The high hydrophilicity of the  $\text{Ca}^{2+}$ -cross-linked alginate makes it less capable of vitronectin adsorption, while the more hydrophobic  $\text{Fe}^{3+}$ -Alg, demonstrated enhanced vitronectin adsorption.<sup>152</sup> This conclusion was further supported by the measurements of wettability and roughness of both  $\text{Ca}^{2+}$  and  $\text{Fe}^{3+}$  cross-linked alginate hydrogels.<sup>71</sup> The obtained results demonstrated that the  $\text{Fe}^{3+}$ -Alg is a promising alternative to the  $\text{Ca}^{2+}$ -cross-linked alginate hydrogel, improving cell adhesion and growth. In addition, harvesting and retrieving of cultured cells can be easily achieved by the dissolution of the alginate matrix using chelating agents such as citrate.<sup>154</sup> Furthermore, the  $\text{Fe}^{3+}$ -Alg was used as a scaffold for 3D growth of cells.<sup>155</sup> Cells were viable inside the matrix up to 14 days after cultivation.

In addition to cell growth, the  $\text{Fe}^{3+}$ -Alg hydrogels have been employed for other biomedical applications, typically in combination with other materials. For example, the combination of hyaluronic acid (HA) and the  $\text{Fe}^{3+}$ -Alg hydrogel has found useful applications. On one hand, injectable hydrogels with shear-thinning and antimicrobial activities were developed and

the release of  $\text{Fe}^{3+}$  ions lead to potential long-term treatment of different bacteria, such as *Escherichia coli* or *Staphylococcus aureus*.<sup>156</sup> On the other hand, HA- $\text{Fe}^{3+}$ -Alg hydrogels showed excellent biocompatibility in a mesothelium cell line and efficacy in reducing adhesion formation in a rat model.<sup>157</sup> Alginate-acrylamide hybrid gels cross-linked with ferric ions showed biocompatibility and promising results for tissue engineering.<sup>158</sup> Chondrogenic cells were successfully grown in this matrix. Remarkably, a 2-fold increase in the production of sulfated glycosaminoglycans was found in the hydrogels when irradiated by light. Additionally, polypyrrole-containing  $\text{Fe}^{3+}$ -Alg demonstrated excellent photothermal conversion properties enabling effective tumor hyperthermia treatment in mice.<sup>159</sup>

### 3.5. Environmental remediation

**3.5.1. Organic dye degradation.** Every year, the production of tons of dyes, mainly for textile, paper and cosmetic industries, generates immense amounts of polluted wastewater.<sup>160</sup> The harmful effects of dyes on health and the environment have attracted interest in developing water treatment technologies.<sup>161</sup> Among these techniques, Advanced Oxidation Processes (AOPs) provide an effective and less expensive strategy to degrade dyes under mild pressure and temperature conditions.<sup>162</sup> AOPs employ free radicals for an electrophilic attack of organic pollutants resulting in  $\text{CO}_2$ ,  $\text{H}_2\text{O}$  and salts.<sup>163</sup> The Fenton reaction of iron ions ( $\text{Fe}^{2+}/\text{Fe}^{3+}$ ) and  $\text{H}_2\text{O}_2$  is an effective approach for hydroxyl free radicals ( $\cdot\text{OH}$ ) production. Drawbacks in the application of the Fenton reactions are the limited pH range (pH 2–4) and the difficulty and cost of iron recovery from the solution.<sup>164</sup> Different approaches using materials such as fibrous polymers,<sup>165</sup> Nafion membranes<sup>166</sup> or clays<sup>167</sup> have been explored to immobilize iron ions and overcome these limitations. Among other materials, the  $\text{Fe}^{3+}$ -Alg hydrogel beads were successfully used as the immobilization matrix for  $\text{Fe}^{3+}$  cations as a heterogeneous dye degradation catalyst.<sup>168</sup> Orange II dye was degraded in less than an hour in the presence of  $\text{H}_2\text{O}_2$  and the  $\text{Fe}^{3+}$ -Alg beads at nearly neutral or slightly acidic pH values (pH 7.8 and pH 5.6). Even faster degradation kinetics was obtained under visible light irradiation<sup>169</sup> (photo-Fenton reaction<sup>170</sup>). Notably, control experiments have clearly demonstrated that the presence of  $\text{H}_2\text{O}_2$  was insufficient for the dye decolorization in the absence of the  $\text{Fe}^{3+}$ -Alg beads, thus, confirming the mechanism of the decolorization process as the photo-Fenton reaction. The photo-Fenton decolorization reaction rate was slower as the number of azo units in the dye increases and the degradation was accelerated by increasing the light irradiation intensity.

In other experiments,  $\text{Fe}^{3+}$ -Alg hydrogel films were employed by Quadrado and coworkers for decolorization of azo Methyl Orange dye.<sup>64</sup> The films were reused in five consecutive degradation cycles with a slight efficiency decrease. The authors reported an optimal concentration of 1 mM  $\text{H}_2\text{O}_2$  while higher concentrations of  $\text{H}_2\text{O}_2$  resulted in loss of degradation efficiency. One could expect that the higher concentration of  $\text{H}_2\text{O}_2$  the faster would be the dye decolorization. However, at greater concentrations of  $\text{H}_2\text{O}_2$ , the free radical formation ( $\cdot\text{OH}$ ) can be

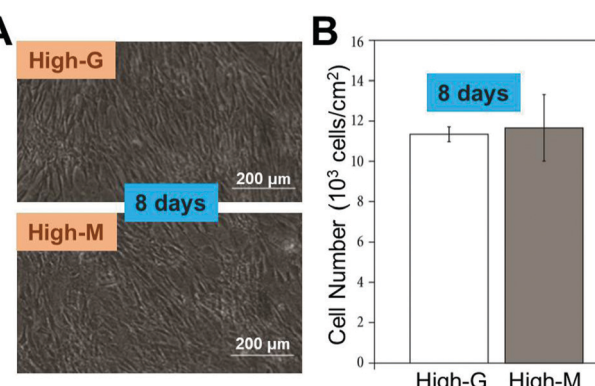


Fig. 10 (A) Proliferation of HDF on  $\text{Fe}^{3+}$ -Alg films under stable gel conditions. (B) Cell number in both High-G and High-M  $\text{Fe}^{3+}$ -Alg films composed of mostly G and M units in the alginate polymer, respectively (adapted from ref. 151 with permission).



hindered and  $\text{H}_2\text{O}_2$  decomposes faster into  $\text{H}_2\text{O}$  and  $\text{O}_2$ .<sup>171</sup> In addition, larger amounts of hydroperoxyl radicals ( $\cdot\text{OOH}$ ) with lower oxidizing strength might be formed.<sup>172</sup> In a similar study,  $\text{Fe}^{3+}$ -Alg hydrogel fibers were employed as heterogeneous catalyst in the photo-Fenton degradation of Reactive Red 195 dye. The dye degradation was achieved in a wide range of pH 3–9 being faster at acidic pH values. The  $\text{Fe}^{3+}$ -Alg hydrogel fibers were used in four degradation cycles without diminishing decolorization rates.<sup>173</sup>

The use of  $\text{H}_2\text{O}_2$  is limited by its instability when it is in contact with other chemical species, particularly in wastewater containing multiple residues. The electro-Fenton process<sup>174</sup> is based on continuous electrochemical generation of  $\text{H}_2\text{O}_2$  to perform the Fenton reaction without the need for  $\text{H}_2\text{O}_2$  added to the bulk solution. Fig. 11A shows the schematic representation of the electro-Fenton dye degradation using  $\text{Fe}^{3+}$ -Alg beads as the  $\text{Fe}^{3+}$  ion source. The  $\text{H}_2\text{O}_2$  is produced *via* oxygen reduction by bubbling compressed air near the cathode.  $\text{H}_2\text{O}_2$  reacts with  $\text{Fe}^{2+}$  electrochemically produced by reduction of  $\text{Fe}^{3+}$  ions leaked from the  $\text{Fe}^{3+}$ -Alg hydrogel. The Fenton reaction results in free hydroxyl radicals ( $\cdot\text{OH}$ ) that induce dye degradation. Decolorization of dyes under electro-Fenton process<sup>174</sup> using  $\text{Fe}^{3+}$ -Alg beads has been extensively studied by Sanromán *et al.*<sup>175–177</sup> Lissamine Green B and Azure B were degraded faster using  $\text{Fe}^{3+}$ -Alg beads as a source of the  $\text{Fe}^{3+}/\text{Fe}^{2+}$  ions than by free iron ions added in the system (Fig. 11B).<sup>175</sup> Dyes were degraded in a wide pH range (pH 2–8), degrading faster at acidic pH. The  $\text{Fe}^{3+}$ -Alg beads were reused in 3 cycles, but the time needed for total dye degradation was increased after each cycle, reflecting the decreasing catalytic activity of the  $\text{Fe}^{3+}$ -Alg beads, probably because of decreasing the  $\text{Fe}^{3+}$  content in the beads. Electro-Fenton oxidation was carried out successfully in a continuous airlift reactor at 3 V and pH 2.<sup>177</sup> However, the system faces a major challenge such as the vigorous agitation of the reactor which promotes  $\text{Fe}^{3+}$  leakage and hydrogel breakage.

It has been demonstrated that several dye degradation processes can be performed in a wide range of pH values

(pH 2–9) using the  $\text{Fe}^{3+}$ -Alg catalyst. This feature has an important environmental implication since most of the residual water from textile industries (pH 7–8) has to be acidified in order to carry out efficiently traditional Fenton reactions, while the acidification is not needed when the  $\text{Fe}^{3+}$ -Alg catalyst is applied. The use of the  $\text{Fe}^{3+}$ -Alg catalyst allows a more economical way for water treatment. In addition to the degradation of dyes,  $\text{Fe}^{3+}$ -Alg hydrogels have been found to be useful for the catalytic degradation of Bisphenol A in aqueous solutions.<sup>178</sup> The  $\text{Fe}^{3+}$ -Alg hydrogels in the form of beads, fibers, and films have noticeable reusability and are easy to handle and remove from solutions. However, leakage of  $\text{Fe}^{3+}/\text{Fe}^{2+}$  ions from the catalyst and de-gelation of the  $\text{Fe}^{3+}$ -Alg hydrogel in the presence of  $\text{H}_2\text{O}_2$  may lead to additional contamination of the wastewater and limits the reusability of the catalyst to a few degradation cycles. Nevertheless, straight-forward procedures have been reported for fast and economical treatment of water polluted by organic contaminants using the  $\text{Fe}^{3+}$ -Alg hydrogels as the catalytic species.

**3.5.2. Inorganic contaminant removal.** Water contamination by inorganic compounds is a common problem all over the world. The majority of these contaminants (e.g., compounds containing arsenic, chromium, and selenium) are by-products of industry and agriculture.<sup>179</sup> Particularly, arsenic-containing compounds are the greatest mass-poisoning contaminants in the world. The impact of arsenic on health is well known and it is associated with several diseases.<sup>180</sup> Chromium contamination, specially Cr(vi), can cause a wide range of liver and kidney damage, as well as respiratory problems.<sup>181</sup> Exposure to selenium over a large period of time is known to have adverse effects, such as the loss of feeling.<sup>182</sup> Techniques for detection, quantification and treatment of these contaminants and others are in the scope of the investigation and numerous applications. Water purification processes based on adsorption/absorption including biochar,<sup>183</sup> magnetic assistance,<sup>184</sup> nanomaterials,<sup>185</sup> clay minerals,<sup>186</sup> and others<sup>179,187</sup> have been reported and are currently in use.<sup>188</sup>

Among these techniques, biomaterials show promising perspectives in cost-effective removal of contaminants from water

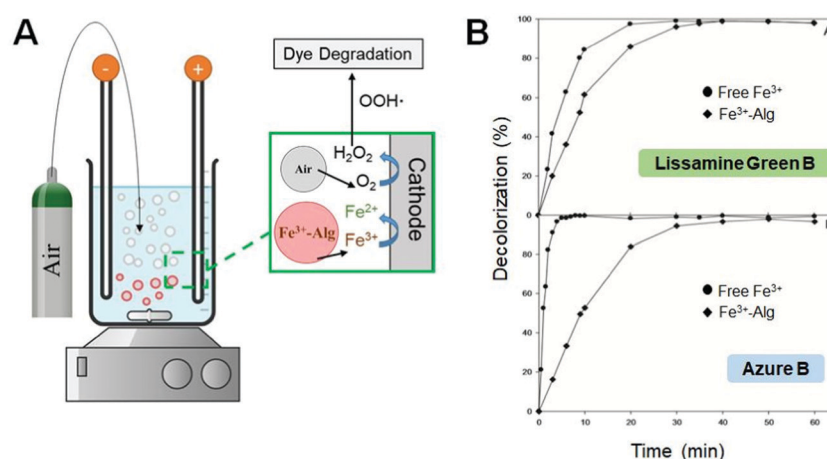


Fig. 11 (A) Schematic representation of an electro-Fenton set up for dye degradation using  $\text{Fe}^{3+}$ -Alg as a catalyst. (B) Degradation of Lissamine Green B and Azure B dyes in the presence of free (in solution)  $\text{Fe}^{3+}$  and  $\text{Fe}^{3+}$ -Alg hydrogel (adapted from ref. 175. Copyright 2012 Elsevier).

resources.<sup>189</sup> Calcium-alginate hydrogel has been employed in water treatment for cesium,<sup>190</sup> herbicides,<sup>191</sup> copper,<sup>192,193</sup> arsenic<sup>192</sup> and lead<sup>193</sup> removal. Sorption and removal of different water contaminants using various ionotropic alginate hydrogels, particularly using  $\text{Fe}^{3+}$ -Alg, were studied.<sup>194,195</sup> The comprehensive study included sorption of As(v)-ionic derivatives (arsenates) by alginate hydrogel beads cross-linked with various metal cations:  $\text{Cu}^{2+}$ ,  $\text{Ca}^{2+}$ ,  $\text{Fe}^{3+}$ , and mixed  $\text{Ca}^{2+}/\text{Fe}^{3+}$ . The synthesis of the latter was carried out by partial exchange of  $\text{Ca}^{2+}$  ions by  $\text{Fe}^{3+}$  ions (Fig. 12A).<sup>196</sup> After 2 hours,  $\text{Fe}^{3+}$ -cross-linked alginate and  $\text{Ca}^{2+}/\text{Fe}^{3+}$ -cross-linked alginate demonstrated similar adsorption of As(v) ions, but after 24 hours the uptake of As(v) ions was reproducibly larger by the mixed- $\text{Ca}^{2+}/\text{Fe}^{3+}$ -cross-linked alginate. Under similar conditions, alginate hydrogels cross-linked with  $\text{Ca}^{2+}$  and  $\text{Cu}^{2+}$  ions did not exhibit remarkable As(v) sorption (Fig. 12B),<sup>194</sup> thus clearly demonstrating the advantage of the  $\text{Fe}^{3+}$ -containing alginate hydrogels. In a recent study, arsenate removal efficiencies close to 80% were obtained using  $\text{Fe}^{3+}$ -Alg beads, while  $\text{Ca}^{2+}$ -Alg showed poor removal performance.<sup>197</sup>

Sorption of Se(iv) and Cr(vi) ions by the mixed- $\text{Ca}^{2+}/\text{Fe}^{3+}$ -cross-linked alginate hydrogel beads was reported.<sup>195</sup> The removal of Se(iv) ions was comparable with that of As(v) ions, whereas the rate of sorption of Cr(vi) ions was slower and less efficient. The effect of Se(iv), As(v) and Cr(vi) ions competition was analyzed in terms of their sorption by  $\text{Fe}^{3+}$ -Alg.<sup>195</sup> With the same concentration level, removal of As(v) ions and Se(iv) ions remained unaffected by Cr(vi) ions, but on the other hand, the sorption of the latter was reduced by 50% by either As(v) and Se(iv) ions. The competition for sorption between Se(iv) and Cr(vi) ions was obtained due to the similar binding strength of these ions. Similarly, but with different final applications,  $\text{Fe}^{3+}$ -

Alg hydrogels have been employed for phosphate<sup>198</sup> and nutrient capture.<sup>199</sup> These results demonstrated the possible use of the  $\text{Fe}^{3+}$ -Alg for agricultural applications.

The literature is consistent with the effects of pH in contaminant removal by ionotropic alginate hydrogels. At very acidic pH < 3, the protonation of uronic moieties in alginate decreases the available binding sites. Indeed, the neutral (protonated) sites do not keep  $\text{Fe}^{3+}$  cations, which are responsible for the sorption of anionic concomitants. In addition, the formation of neutral species of soluble concomitants (e.g.,  $\text{H}_3\text{AsO}_4$ ,  $\text{H}_2\text{SeO}_3$ ) may inhibit their sorption at low pH.<sup>195,196</sup> At basic pH values, the removal efficiency is decreased due to the instability of ionotropic alginate hydrogels. The optimal pH value was found to be pH ca. 4, with a suitable  $\text{Fe}^{3+}$  ion leakage/contaminant removal ratio.<sup>195</sup> Overall, while the contaminant removal might be efficient enough, particularly with  $\text{Fe}^{3+}$ -containing alginate hydrogels, the exact mechanism of the sorption process requires additional studies.

### 3.6. Material science

**3.6.1. Composite materials.** Composite hydrogel materials are produced from two or more individual materials. The major goal of combination of materials is to improve the properties of the original materials, such as porosity, stimuli-responsiveness, stability or mechanical strength. The individual materials can be chemically bound to each other (e.g., upon cross-linking<sup>200</sup>), electrostatically bound (e.g., produced by the layer-by-layer deposition<sup>201</sup>), or physically interpenetrated between polymeric chains (interpenetrating polymer networks<sup>117</sup>), or integrated by many other unconventional means.<sup>11</sup>  $\text{Fe}^{3+}$ -Alg has been combined with different materials to improve its properties and enhance its performance.

Polyacrylamide interpenetrated in  $\text{Fe}^{3+}$ -Alg has been a widely exploited composite for photoresponsive shape memory material,<sup>202</sup> increasing hydrogel stiffness<sup>70,148</sup> stretchability and toughness.<sup>203</sup> Poly(*N*-isopropylacrylamide) was physically interpenetrated into  $\text{Fe}^{3+}$ -Alg hydrogel conferring it with thermo- and magnetic-responsive capabilities.<sup>204</sup> An increase in the iron concentration leads to a significant decrease in pore size and improve in the deswelling rates of the hydrogel. Polypyrrole-containing alginate was used for tumor hyperthermia treatment.<sup>159</sup> The ability of  $\text{Fe}^{3+}$  ions to synchronously induce gelatinization of alginate and polymerization of pyrrole endowed the material with superior photothermic conversion properties.

The surface porosity of  $\text{Fe}^{3+}$ -Alg hydrogel was significantly reduced after deposition of a polyethylenimine (PEI) layer cross-linked to carboxylic groups at the surface of  $\text{Fe}^{3+}$ -Alg hydrogel (Fig. 13).<sup>127</sup> The PEI-alginate composite showed enhanced retention of DNA preventing its premature leakage from the hydrogel. (Fig. 13). Additionally, the incorporation of gold nanoparticles to the hydrogels produced a nanocomposite hydrogel with stimuli-responsive characteristics.<sup>127</sup> A carbon dot- $\text{Fe}^{3+}$ -Alg nanocomposite leads to higher absorption in the UV-region showing the potential use of this material for UV-shielding.<sup>205</sup> Similarly, cross-linking of sodium alginate with ferric ions containing ethylenediaminetetraacetic

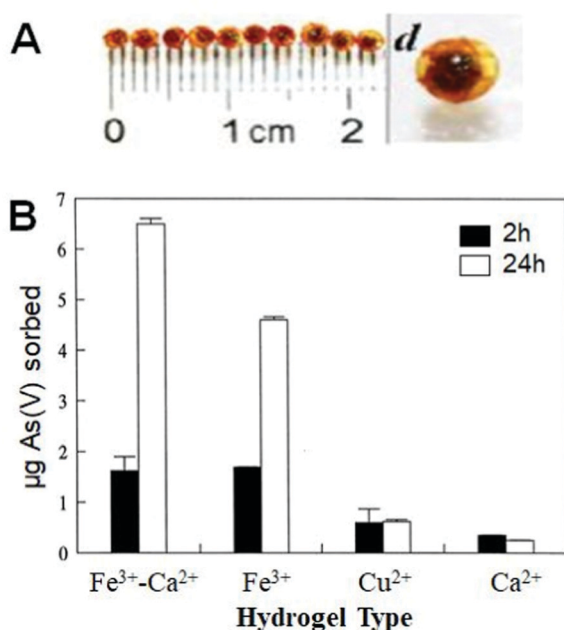
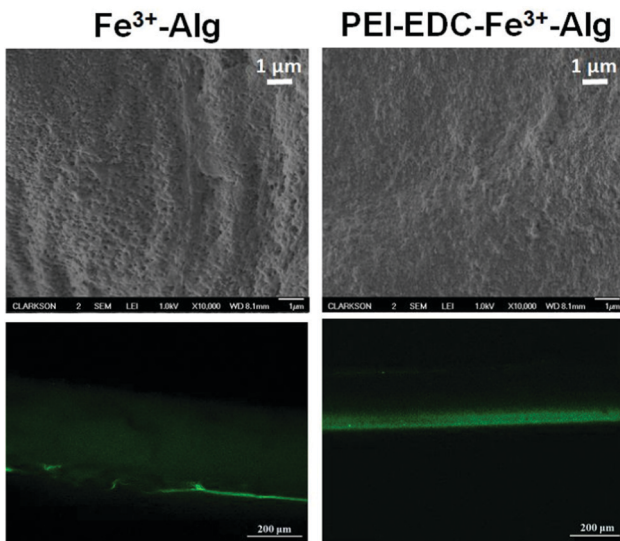


Fig. 12 (A) Visual appearance of mixed- $\text{Ca}^{2+}/\text{Fe}^{3+}$ -Alg beads. (B) As(v) sorption using different ionotropic alginate hydrogels (adapted from ref. 194. Copyright 1998 Elsevier).





**Fig. 13** Scanning electron (top) and fluorescent confocal microscope (bottom) images of a plain  $\text{Fe}^{3+}$ -Alg and PEI-cross-linked alginate hydrogel (PEI-EDC- $\text{Fe}^{3+}$ -Alg) (adapted from ref. 127. Copyright 2020 American Chemical Society).

acid (EDTA) incorporated within the hydrogel leads to enhanced mechanical properties and flatter and densely packed structure with higher thermal stability.<sup>87</sup> These properties were necessary for the intended application of the material as UV shielding films.

$\text{Fe}^{3+}$ -Alg was blended with carboxymethyl chitin prior cross-linking with iron ions.<sup>69</sup> As a result, longer stability and sustained release were achieved in phosphate solutions. A hyaluronic acid (HA) and poly(allylamine hydrochloride) (PAH) layer-by-layer deposition technique was employed to produce photo-responsive PAH/HA/ $\text{Fe}^{3+}$ -Alg nanogels.<sup>110</sup> The complexation occurring between PAH and alginate chains hindered the burst release of folic acid that was released in a controlled manner upon light irradiation. Nanofibrous  $\text{Fe}^{3+}$ -Alg strips were synthesized by their combination with polyacrylonitrile (PAN) for tetracycline (TC) visual detection.<sup>206</sup>

The sensor is based on the complexation of TC with  $\text{Fe}^{3+}$  which results in a color change easily detected by the naked eye. The sensing strips allowed fast sensing of TC with the possibility to reuse them in 6 detection cycles.

**3.6.2. Patterning.** Alginate hydrogels biocompatibility and biodegradability make them an ideal biomaterial for regenerative medicine and tissue engineering.<sup>61</sup> For such biomedical applications, the control of the spatial and temporal organization of the polymer without compromising its properties is one of the main challenges.<sup>207,208</sup> Patterning alginate at different length scales is fundamental for *in vivo* applications as it will allow superior control of the processes occurring in the hydrogel, such as cell growth and leakage of entrapped species.  $\text{Ca}^{2+}$ -Alg patterning strategies are available in the literature.<sup>209,210</sup> The already mentioned mechanical and responsive properties of  $\text{Fe}^{3+}$ -Alg hydrogel have been exploited for patterning of this gel. Photo-patterning is a powerful method for producing hydrogels of specific shapes.  $\text{Fe}^{3+}$ -Alg hydrogel containing lactate was irradiated with light selectively through a mask.<sup>84</sup> After the dissolution of the irradiated area, the solution was removed obtaining a patterned  $\text{Fe}^{3+}$ -Alg film (Fig. 14A). Then, the patterned  $\text{Fe}^{3+}$ -Alg film was immersed in a 50 mM  $\text{CaCl}_2$  and 50 mM ascorbic acid solution, exchanging the  $\text{Fe}^{3+}$  gelling ions for  $\text{Ca}^{2+}$  ions (Fig. 14B).<sup>211</sup> Since  $\text{Ca}^{2+}$ -cross-linked alginate cannot be directly photo-patterned because it lacks photochemical properties, the patterning can be done with the  $\text{Fe}^{3+}$ -Alg, then converting it to the  $\text{Ca}^{2+}$ -cross-linked hydrogel by the cation exchange. Photo-patterning of  $\text{Fe}^{3+}$ -Alg allowed the creation of gradients and interfaces in stiffness and elasticity (Fig. 14C).<sup>158,212</sup> In addition, the photo-dissociable  $\text{Fe}^{3+}$ -Alg coordination was used as a molecular switch to realize photo-control of shape memory on both macroscopic and microscopic scales and enable a number of other functions.<sup>202</sup>  $\text{Fe}^{3+}$ -Alg films with complex shapes have been fabricated using templates of patterned paper.<sup>213</sup> Chromatography paper was cut with a laser cutter and wetted with the gelling ion solution. The addition of alginate solution resulted in gel formation with the template shape (Fig. 14D).

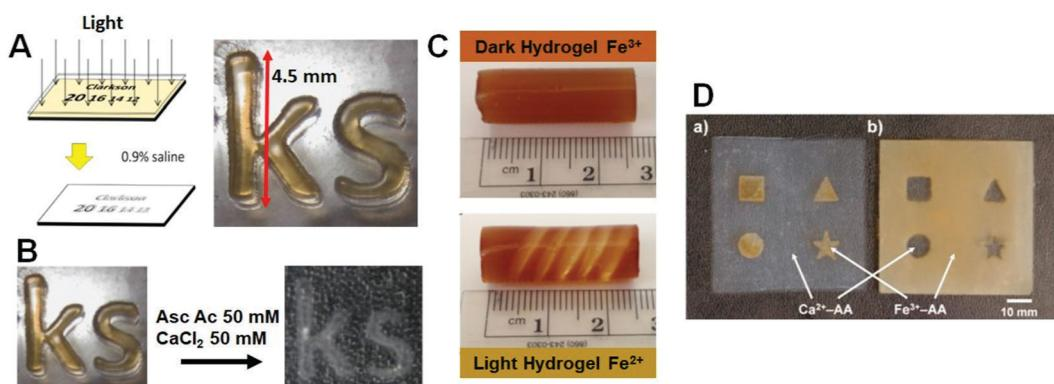


**Fig. 14** (A)  $\text{Fe}^{3+}$ -Alg hydrogel photo-patterned (adapted from ref. 84 with permission); (B) the same hydrogel after exchange of  $\text{Fe}^{3+}$  for  $\text{Ca}^{2+}$  cations (adapted from ref. 211. Copyright 2015 Elsevier); (C)  $\text{Fe}^{3+}$ -Alg hydrogel photo-patterned (adapted from ref. 212. Copyright 2015 American Chemical Society). (D)  $\text{Fe}^{3+}$ -Alg and  $\text{Ca}^{2+}$ -Alg growth on templates with different shapes (adapted from ref. 213. Copyright 2009 American Chemical Society).

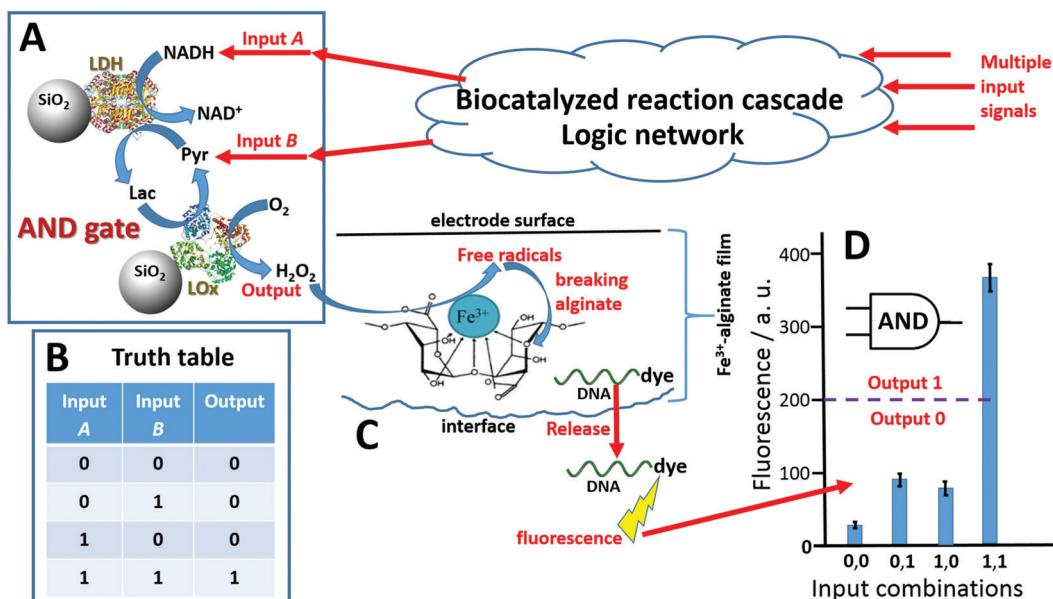


**Fig. 15** (A) The biocatalytic cascade is catalyzed by two enzymes, lactate dehydrogenase (LDH) and lactate oxidase (Lox), yielding  $\text{H}_2\text{O}_2$  when both input signals, NADH and pyruvate (Pyr), are present. (B) The truth table corresponding to the Boolean AND logic gate. Note that the output signal 1 (corresponding to the  $\text{H}_2\text{O}_2$  production) appears only in the presence of both input signals (1, 1 input combination). (C) Alginate film decomposition and the DNA molecules release due to the formation of free radicals through a Fenton-type reaction catalyzed by iron cations. (D) Fluorescence analysis of the DNA release (note that it was labeled with a fluorescent dye) upon application of the input signals in different combinations (adapted from ref. 10. Copyright 2020 Elsevier.)

### 3.7. Boolean logic operations performed for controlling biomolecule release – Integration of unconventional computing and actuation

Various types of signal-switchable chemical systems have been recently designed for realizing molecule<sup>214</sup> and biomolecule<sup>215</sup> computing in the general framework of unconventional computing.<sup>216</sup> Among many other biochemical systems,<sup>136</sup> used for biomolecule computing, sophisticated enzyme systems<sup>145,217,218</sup> allowed functional integration of logic operations with actuation functions. These enzyme-based Boolean logic gates allowed control of bioelectronic systems<sup>219</sup> and molecule-release systems<sup>106</sup> with logically processed biomolecule input signals. Logic control of payload from the  $\text{Fe}^{3+}$ -Alg hydrogel represents one of the systems where the release function is activated with a number of chemical input signals processed by biocatalytic reactions.<sup>144</sup> Silica nanoparticles ( $\text{SiO}_2$ , *ca.* 200 nm diameter) were chemically functionalized with different enzymes and then they were entrapped into an  $\text{Fe}^{3+}$ -Alg hydrogel films prepared electrochemically<sup>47</sup> at an electrode surface. The  $\text{SiO}_2$  nanoparticles holding the enzymes and inhibiting their leakage from the hydrogel represent a convenient platform for immobilization of catalytically active enzymes. Fig. 15A shows a reaction cascade catalyzed by lactate dehydrogenase (LDH) and lactate oxidase (Lox) producing  $\text{H}_2\text{O}_2$  as the reaction output. The input signals, NADH (Input A) and pyruvate (Pyr; Input B) were applied in four different combinations (0, 0; 0, 1; 1, 0; 1, 1) where logic value 0 corresponded to the input absence (physically zero concentration) and logic value 1 was defined as an experimentally optimized concentration of the input chemicals. In order to complete the cascade and produce the  $\text{H}_2\text{O}_2$  output, both inputs must be present in the system (1, 1 input combination), thus

mimicking a Boolean AND logic gate, Fig. 15B. When  $\text{H}_2\text{O}_2$  was produced, the  $\text{Fe}^{3+}$ -Alg hydrogel film was decomposed in a Fenton-type reaction catalyzed by iron cations yielding free radicals and decomposing the alginate polymer chains,<sup>105</sup> Fig. 15C. This resulted in the release of DNA molecules entrapped in the film. The released DNA molecules were analyzed optically (note that they were labeled with a fluorescent dye for a convenient analysis), Fig. 15D. A similar approach was used to perform different logic operations (e.g., Boolean OR logic gate) with the use of different combinations of molecule inputs and different enzymes catalyzing reactions inside the alginate film.<sup>144</sup> The system complexity can be significantly increased by assembling a reaction cascade catalyzed by many enzymes and activated by a larger number of biomolecule input signals. These processes based on multi-step catalytic reactions can mimic Boolean logic operations of high complexity, leading to DNA computers, nano-machines and nano-robots.<sup>220</sup>

## 4. Conclusions and perspectives

As it was already noted in the introduction, stimuli-responsive hydrogels are very important functional materials, which can find numerous applications in various areas of science and technology, particularly in biomedical applications.<sup>10</sup> Depending on the properties of specific polymeric materials, the hydrogels can respond to different input signals, physical or chemical, triggering gel-sol transition and releasing a preloaded cargo molecules or nanospecies. On the other hand, the opposite process, the sol-gel transition, can be triggered in the presence of specific cross-linkers or upon changing the environment (e.g., temperature, pH, etc.). While many synthetic polymers have been



extensively studied for reversible signal-triggered sol-gel transformations, the natural polymers, and among them alginate, have demonstrated unique mechanical, physical and chemical features, which are especially important for biomedical applications, including signal-triggered drug release. While biocompatibility of alginate is particularly important for biomedical applications,<sup>33</sup> operating as implantable or externally wearable materials, much broader applications in technology have emerged.<sup>221</sup> For example, signal-switchable hydrogels (synthetic or natural, including alginate), have been extensively used for creation of signal-switchable interfaces and modified electrodes.<sup>222</sup> Novel unusual applications in biocomputing became possible due to signal-triggered changes in the alginate structure and properties. The important part of the signal-controlled hydrogel structure is a cross-linker that is responsible for the sol-gel transformation. Notably, different metal cations can operate as cross-linkers, each kind of cations with a different functionality. Iron cations ( $\text{Fe}^{2+} \leftrightarrow \text{Fe}^{3+}$ ) possess particularly rich functions changed upon redox transformations, which can be produced chemically, electrochemically, and photochemically. Overall, iron-cross-linked alginate hydrogels have particularly unique properties and ability to respond reversibly to various external signals in biological environments.

The unique features of  $\text{Fe}^{3+}$ -Alg originate from the particular chemistry of  $\text{Fe}^{3+}$  cations and their exclusive binding to alginate polymer chains. For this reason, an increasing interest in this material has been noted in the number of publications, primarily in the last decade.<sup>223–234</sup>  $\text{Fe}^{3+}$ -Alg can be synthesized from nm to mm scale with different arrangements (e.g., beads, films, electrodeposited layers). In addition, the hydrogel can be degraded by different mechanisms providing the material with stimuli-responsive and patterning capabilities. The stimulus-responsiveness of  $\text{Fe}^{3+}$ -Alg hydrogels has been by far the most appealing feature. It is important to mention that despite the vast amount of responsive materials available, it is uncommon to find those with multiple-responsiveness. Signals, including  $\text{H}_2\text{O}_2$ , light, pH or electric potential, have been demonstrated to induce hydrogel dissolution and release any encapsulated (bio)-molecules and various species (e.g., proteins, nanoparticles, small molecules, etc.) demonstrating “smart” drug delivery processes. The enhanced mechanical properties compared to other ionotropic alginates hydrogels represent an advantage for practical applications in which softer alginate hydrogels are known to have poor performance. Furthermore, the higher hydrophobicity of  $\text{Fe}^{3+}$ -Alg has been exploited for enhanced cell adhesion and growth as well as for contaminant removal.

It should be noted that iron cations, particularly in composition of complex biomolecules, have very important biological functions.<sup>235,236</sup> Therefore, the release of  $\text{Fe}^{2+}$  cations to biofluids upon dissolution of  $\text{Fe}^{3+}$ -Alg hydrogels may result in physiological changes, which must be considered when biomedical (particularly implantable or invasive) applications are planned.

The use of  $\text{Fe}^{3+}$ -Alg hydrogels, particularly in biomedical applications, has obvious advantages and disadvantages, which in a large extent depend on specific goals and applications.

Particularly, the use of Fenton-type reactions producing free radicals for decomposing the alginate matrices and stimulating biomolecule cargo release may result in damaging releasing biomolecules. For example, it has been shown that the DNA released from an alginate hydrogel shows damages because of the catalytically produced oxidative free radicals.<sup>144</sup> To avoid this damage, the loaded DNA was included in a protecting shell. The advantage of the  $\text{Fe}^{3+}$ -Alg hydrogel is its responsiveness to various signals. On the other hand, while it can be dissolved upon application of different signals and their combinations, the hydrogel dissolution and molecule release may proceed non-specifically by a signal which is not properly planned.

Despite the enormous potential of  $\text{Fe}^{3+}$ -Alg hydrogels, their real-life applications are far from now. In our opinion, the following steps have to be done to achieve the practical use of this interesting material: (i) greater efforts need to be done to understand the mechanism by which  $\text{Fe}^{3+}$  cations coordinate to alginate and other polysaccharides; (ii) mass production of alginate hydrogels is known to be complicated and their heterogeneity have to be addressed to obtain higher reproducibility. This is essential for a better understanding of their behavior in *in vivo* biomedical applications or environmental applications. For these applications, (iii) it will be required to increase the stability of the hydrogel specifically in environments with high ionic strength, such as biological fluids or residual waters and (iv) enhance the mechanical properties of the hydrogel. The solution to this can be found by the combination of  $\text{Fe}^{3+}$ -Alg with other materials forming composites. As it has been shown before, composite materials using  $\text{Fe}^{3+}$ -Alg are a promising alternative to overcome hydrogels disadvantages and add novel features to the system. In particular, novel advanced materials (metal organic frameworks, graphene, carbon nanotubes or quantum dots) in combination with alginate hydrogels will open several new paths towards smarter, economic and sustainable materials.

Nevertheless, with this review paper, the authors pretend to promote research related with this fascinating material by providing the most updated summary of the properties and highlighting the state-of-the-art of the  $\text{Fe}^{3+}$ -Alg hydrogels.

## Data availability statement

The present article is a review of published materials originating from many research groups.

## The list of abbreviations (additional abbreviations are explained in figure captions)

AOPs	Advanced oxidative processes
$\beta$ -Amy	$\beta$ -Amylase (enzyme)
$\text{Ba}^{2+}$ -Alg	Barium-cross-linked alginate hydrogel
BSA	Bovine serum albumin (protein)
$\text{Ca}^{2+}$ -Alg	Calcium-cross-linked alginate hydrogel



EDC	1-Ethyl-3-(3-dimethylaminopropyl)carbodiimide (carbodiimide coupling reagent)
EDTA	Ethylenediaminetetraacetic acid (chelating agent)
Fe <sup>3+</sup> -Alg	Fe <sup>3+</sup> -cross-linked alginate hydrogel
G	$\alpha$ -L-Guluronate
Glc	Glucose
GlcA	Gluconic acid (product of enzymatic glucose oxidation)
HA	Hyaluronic acid
HDF	Human dermal fibroblasts (main cell type present in skin connective tissue)
Lac	Lactate
LDH	Lactate dehydrogenase (enzyme)
LOx	Lactate oxidase (enzyme)
M	$\beta$ -D-Mannuronate
MPh	Maltose phosphorylase (enzyme)
NAD <sup>+</sup> /NADH	Nicotinamide adenine dinucleotide (oxidized/reduced forms)
NaAlg	Sodium alginate
NPs	Nanoparticles
PAH	Poly(allylamine hydrochloride)
PBS	Phosphate-buffered saline
PEI	Polyethyleneimine
PQQ	Pyrroloquinoline quinone
PQQ-GDH	PQQ-dependent glucose dehydrogenase (enzyme)
Pyr	Pyruvate
TC	Tetracycline

## Conflicts of interest

The authors declare no conflict of interest.

## Acknowledgements

The authors thank Human Frontiers Science Program for funding through grant RGP0002/2018.

## References

- 1 *Hydrogels – Recent Advances*, ed. V. K. Thakur and M. K. Thakur, Springer, Berlin, 2018.
- 2 X. Du, J. Zhou, J. Shi and B. Xu, Supramolecular hydrogelators and hydrogels: From soft matter to molecular biomaterials, *Chem. Rev.*, 2015, **115**, 13165–13307.
- 3 J. Saroia, W. Yanen, Q. Wei, K. Zhang, T. Lu and B. Zhang, A review on biocompatibility nature of hydrogels with 3D printing techniques, tissue engineering application and its future prospective, *Bio-Des. Manuf.*, 2018, **1**, 265–279.
- 4 O. Jeon, K. H. Bouhadir, J. M. Mansour and E. Alsberg, Photocrosslinked alginate hydrogels with tunable biodegradation rates and mechanical properties, *Biomaterials*, 2009, **30**, 2724–2734.
- 5 C. K. Thota, N. Yadav and V. S. Chauhan, A novel highly stable and injectable hydrogel based on a conformationally restricted ultrashort peptide, *Sci. Rep.*, 2016, **6**, 31167.

- 6 F. Ullah, M. B. H. Othman, F. Javed, Z. Ahmad and H. M. Akil, Classification, processing and application of hydrogels: A review, *Mater. Sci. Eng., C*, 2015, **57**, 414–433.
- 7 Q. Chai, Y. Jiao and X. Yu, Hydrogels for biomedical applications: Their characteristics and the mechanisms behind them, *Gels*, 2017, **3**, 6.
- 8 J. Li and D. J. Mooney, Designing hydrogels for controlled drug delivery, *Nat. Rev. Mater.*, 2016, **1**, 16071.
- 9 K. Y. Lee and D. J. Mooney, Hydrogels for tissue engineering, *Chem. Rev.*, 2001, **101**, 1869–1880.
- 10 K. Kaniewska, M. Karbarz and E. Katz, Nanocomposite hydrogel films and coatings – Features and applications, *Appl. Mater. Today*, 2020, **20**, 100776.
- 11 X. Zhao, X. Chen, H. Yuk, S. Lin, X. Liu and G. Parada, Soft materials by design: Unconventional polymer networks give extreme properties, *Chem. Rev.*, 2021, **121**, 4309–4372.
- 12 E. M. Ahmed, Hydrogel: Preparation, characterization, and applications: A review, *J. Adv. Res.*, 2015, **6**, 105–121.
- 13 S. Nangia, S. Warkar and D. Katyal, A review on environmental applications of chitosan biopolymeric hydrogel based composites, *J. Macromol. Sci., Part A: Pure Appl. Chem.*, 2018, **55**, 747–763.
- 14 A. Choodum, K. Malathong, N. NicDaeid, W. Limsakul and W. Wongniramaikul, A cost effective hydrogel test kit for pre and post blast trinitrotoluene, *Forensic Sci. Int.*, 2016, **266**, 202–208.
- 15 K. Haraguchi, Nanocomposite hydrogels, *Curr. Opin. Solid State Mater. Sci.*, 2007, **11**, 47–54.
- 16 U. S. K. Madduma-Bandarage and S. V. Madihally, Synthetic hydrogels: Synthesis, novel trends, and applications, *J. Appl. Polym. Sci.*, 2021, **138**, e50376.
- 17 S. J. Buwalda, Bio-based composite hydrogels for biomedical applications, *Multifunct. Mater.*, 2020, **3**, 022001.
- 18 K. Y. Lee and D. J. Mooney, Alginate: Properties and biomedical applications, *Prog. Polym. Sci.*, 2012, **37**, 106–126.
- 19 B. Tian, S. Hua, Y. Tian and J. Liu, Chemical and physical chitosan hydrogels as prospective carriers for drug delivery: A review, *J. Mater. Chem. B*, 2020, **8**, 10050–10064.
- 20 S. M. F. Kabir, P. P. Sikdar, B. Haque, M. A. R. Bhuiyan, M. A. Ali and M. N. Islam, Cellulose-based hydrogel materials: chemistry, properties and their prospective applications, *Prog. Biomater.*, 2018, **7**, 153–174.
- 21 V. Morya, S. Walia, B. B. Mandal, C. Ghoroi and D. Bhatia, Functional DNA based hydrogels: Development, properties and biological applications, *ACS Biomater. Sci. Eng.*, 2020, **6**, 6021–6035.
- 22 K. Roy, G. Pandit, M. Chetia, A. K. Sarkar, S. Chowdhuri, A. P. Bidkar and S. Chatterjee, Peptide hydrogels as platforms for sustained release of antimicrobial and antitumor drugs and proteins, *ACS Appl. Bio Mater.*, 2020, **3**, 6251–6262.
- 23 K. I. Draget, O. Smidsrød and G. Skjåk-Bræk, Alginates from algae, in: *Polysaccharides and Polyamides in the Food Industry. Properties, Production, and Patents*, ed. A. Steinbüchel and S. K. Rhee, Wiley-VCH, Weinheim, 2005.



24 I. Pacheco-Leyva, F. Guevara Pezoa and A. Díaz-Barrera, Alginate biosynthesis in *Azotobacter vinelandii*: Overview of molecular mechanisms in connection with the oxygen availability, *Int. J. Polym. Sci.*, 2016, **2016**, 2062360.

25 Ý. A. Mørch, I. Donati, B. L. Strand and G. Skjak-Bræk, Effect of  $\text{Ca}^{2+}$ ,  $\text{Ba}^{2+}$ , and  $\text{Sr}^{2+}$  on alginate microbeads, *Biomacromolecules*, 2006, **7**, 1471–1480.

26 G. Liling, Z. Di, X. Jiachao, G. Xin, F. Xiaoting and Z. Qing, Effects of ionic crosslinking on physical and mechanical properties of alginate mulching films, *Carbohydr. Polym.*, 2016, **136**, 259–265.

27 N. K. Sachan, S. Pushkar, A. Jha and A. Bhattacharya, Sodium alginate: The wonder polymer for controlled drug delivery, *J. Pharm. Res.*, 2009, **2**, 1191–1199.

28 M. Szekalska, A. Puciłowska, E. Szymańska, P. Ciosek and K. Winnicka, Alginate: Current use and future perspectives in pharmaceutical and biomedical applications, *Int. J. Polym. Sci.*, 2016, **17**, 7697031.

29 R. G. Puscaselu, A. Lobiuc, M. Dimian and M. Covasa, Alginate: From food industry to biomedical applications and management of metabolic disorders, *Polymers*, 2020, **12**, 2417.

30 *Alginates: Biology and Applications, Series: Microbiology Monographs*, ed. B. H. A. Rehm, Springer, Dordrecht, 2009, vol. 13.

31 *Alginates in Drug Delivery*, ed. A. K. Nayak and M. S. Hasnain, Academic Press, Cambridge, MA, 2020.

32 *Alginates – Versatile Polymers in Biomedical Applications and Therapeutics*, ed. M. S. Hasnain and A. K. Nayak, Apple Academic Press, Burlington, Canada, 2019.

33 *Alginates: Applications in the Biomedical and Food Industry*, ed. S. Ahmed, Wiley, Hoboken, NJ, 2019.

34 *Alginates: Production, Types and Applications*, ed. M. E. Molina and A. J. Quiroga, Nova Science Pub., Hauppauge, NY, 2012.

35 E. Ferrari and M. Saladini, Iron(III) complexing ability of carbohydrate derivatives, *J. Inorg. Biochem.*, 2004, **98**, 1002–1008.

36 H. B. Abrahamson, A. B. Rezvani and J. G. Brushmiller, Photochemical and spectroscopic studies of complexes of iron(II) with citric acid and other carboxylic acids, *Inorg. Chim. Acta*, 1994, **226**, 117–127.

37 Z. Wang, N. Liu, F. Feng and Z. Ma, Synthesis of cadmium, lead and copper alginate nanobeads as immunosensing probes for the detection of AFP, CEA and PSA, *Biosens. Bioelectron.*, 2015, **70**, 98–105.

38 L. A. Berner and L. F. Hood, Iron binding by sodium alginate, *J. Food Sci.*, 1983, **48**, 755–758.

39 R. Ray, S. Maity, S. Mandal, T. K. Chatterjee and B. Sa, Studies on the release of ibuprofen from  $\text{Al}^{3+}$  ion cross-linked homopolymeric and interpenetrating network hydrogel beads of carboxymethyl xanthan and sodium alginate, *Adv. Polym. Technol.*, 2011, **30**, 1–11.

40 G. T. Grant, E. R. Morris, D. A. Rees, P. J. C. Smith and D. Thom, Biological interactions between polysaccharides and divalent cations: The egg-box model, *FEBS Lett.*, 1973, **32**, 195–198.

41 L. Li, Y. Fang, R. Vreeker and I. Appelqvist, Reexamining the egg-box model in calcium-alginate gels with X-ray diffraction, *Biomacromolecules*, 2007, **8**, 464–468.

42 P. Sikorski, F. Mo, G. Skjæk-Bræk and B. T. Stokke, Evidence for egg-box-compatible interactions in calcium-alginate gels from fiber X-ray diffraction, *Biomacromolecules*, 2007, **8**, 2098–2103.

43 R. B. Hernández, A. P. Franco, O. R. Yola, A. López-Delgado, J. Felcman, M. A. L. Recio and A. L. R. Mercè, Coordination study of chitosan and  $\text{Fe}^{3+}$ , *J. Mol. Struct.*, 2008, **877**, 89–99.

44 Y. Cao, S. Li, Y. Fang, K. Nishinari, G. O. Phillips, A. Lerbret and A. Assifaoui, Specific binding of trivalent metal ions to  $\lambda$ -carrageenan, *Int. J. Biol. Macromol.*, 2018, **109**, 350–356.

45 K. J. Sreeram, H. Y. Shrivastava and B. U. Nair, Studies on the nature of interaction of iron(III) with alginates, *Biochim. Biophys. Acta*, 2004, **1670**, 121–125.

46 B. Gyuresik and L. Nagy, Carbohydrates as ligands: Coordination equilibria and structure of the metal complexes, *Coord. Chem. Rev.*, 2000, **203**, 81–149.

47 Z. Jin, G. Güven, V. Bocharova, J. Halámek, I. Tokarev, S. Minko, A. Melman, D. Mandler and E. Katz, Electrochemically controlled drug-mimicking protein release from iron-alginate thin-films associated with an electrode, *ACS Appl. Mater. Interfaces*, 2012, **4**, 466–475.

48 T. E. Furia, *CRC Handbook of Food Additives*, CRC Press, Boca Raton, FL, 2nd edn, 1972, vol. 2.

49 A. N. Pham, A. L. Rose, A. J. Feitz and D. White, Kinetics of Fe(III) precipitation in aqueous solutions at pH 6.0–9.5 and 25 °C, *Geochim. Cosmochim. Acta*, 2006, **70**, 640–650.

50 J. M. Nieto, C. Peniche-Covas and J. Del Bosque, Preparation and characterization of a chitosan – Fe(III) complex, *Carbohydr. Polym.*, 1992, **18**, 221–224.

51 S. C. Bathia and N. Ravi, A Magnetic Study of an Fe-chitosan complex and its relevance to other biomolecules, *Biomacromolecules*, 2000, **1**, 413–417.

52 P. Sipos, O. Berkesi, E. Tombacz, T. G. S. Pierre and J. Webb, Formation of spherical iron(III) oxyhydroxide nanoparticles sterically stabilized by chitosan in aqueous solutions, *J. Inorg. Biochem.*, 2003, **95**, 55–63.

53 B. J. Lee, G. H. Min and T. Kim, Preparation and in vitro release of melatonin-loaded multivalent cationic alginate beads, *Arch. Pharmacal Res.*, 1996, **19**, 280–285.

54 C. Menkabi, F. Quignard and T. Mineva, Complexation of trivalent metal cations to mannuronate type alginate models from a density functional study, *J. Phys. Chem. B*, 2016, **120**, 3615–3623.

55 Y. Dong, W. Dong, Y. Cao, Z. Han and Z. Ding, Preparation and catalytic activity of Fe alginate gel beads for oxidative degradation of azo dyes under visible light irradiation, *Catal. Today*, 2011, **175**, 346–355.

56 J. Brus, M. Urbanova, J. Czernek, M. Pavelkova, K. Kubova, J. Vyslouzil, S. Abbrent, R. Konefal, J. Horský, D. Vetchy, J. Vysloužil and P. Kulich, Structure and dynamics of alginate gels cross-linked by polyvalent ions probed via solid state NMR spectroscopy, *Biomacromolecules*, 2017, **18**, 2478–2488.



57 T. Bechtold, A. P. Manian, H. B. Öztürk, U. Paul, B. Široká, J. Široký, H. Soliman, L. T. T. Vo and H. Vu-Manh, Ion-interactions as driving force in polysaccharide assembly, *Carbohydr. Polym.*, 2013, **93**, 316–323.

58 P. Singh, S. K. Singh, J. Bajpai, A. K. Bajpai and R. B. Shrivastava, Iron crosslinked alginate as novel nanosorbents for removal of arsenic ions and bacteriological contamination from water, *J. Mater. Res. Technol.*, 2014, **3**, 195–202.

59 K. I. Draget and C. Taylor, Chemical, physical and biological properties of alginates and their biomedical implications, *Food Hydrocolloids*, 2011, **25**, 251–256.

60 D. R. Sahoo and T. Biswal, Alginate and its application to tissue engineering, *SN Appl. Sci.*, 2021, **3**, 30.

61 J. Sun and H. Tan, Alginate-based biomaterials for regenerative medicine applications, *Materials*, 2013, **6**, 1285–1309.

62 A. D. Augst, H. J. Kong and D. J. Mooney, Alginate hydrogels as biomaterials, *Macromol. Biosci.*, 2006, **6**, 623–633.

63 F. Abasalizadeh, S. V. Moghaddam, E. Alizadeh, E. Akbari, E. Kashani, S. M. B. Fazljou, M. Torbati and A. Akbarzadeh, Alginate-based hydrogels as drug delivery vehicles in cancer treatment and their applications in wound dressing and 3D bioprinting, *J. Biol. Eng.*, 2020, **14**, 8.

64 R. F. N. Quadrado and A. R. Fajardo, Fast decolorization of azo methyl orange via heterogeneous Fenton and Fenton-like reactions using alginate- $\text{Fe}^{2+}/\text{Fe}^{3+}$  films as catalysts, *Carbohydr. Polym.*, 2017, **177**, 443–450.

65 J. Wu, H. Zheng, F. Zhang, R. J. Zeng and B. Xing, Iron-carbon composite from carbonization of iron-crosslinked sodium alginate for Cr(vi) removal, *Chem. Eng. J.*, 2019, **362**, 21–29.

66 P. Veres, D. Sebok, I. Dékány, P. Gurikov, I. Smirnova, I. Fábian and J. Kalmár, A redox strategy to tailor the release properties of Fe(III)-alginate aerogels for oral drug delivery, *Carbohydr. Polym.*, 2018, **188**, 159–167.

67 K. Y. Lee, J. A. Rowley, P. Eiselt, E. M. Moy, K. H. Bouhadir and D. J. Mooney, controlling mechanical and swelling properties of alginate hydrogels independently by cross-linker type and cross-linking density, *Macromolecules*, 2000, **33**, 4291–4294.

68 M. Golmohamadi and K. J. Wilkinson, Diffusion of ions in a calcium alginate hydrogel-structure is the primary factor controlling diffusion, *Carbohydr. Polym.*, 2013, **94**, 82–87.

69 X.-W. Shi, Y.-M. Du, L.-P. Sun, J.-H. Yang, X.-H. Wang and X.-L. Su, Ionically crosslinked alginate/carboxymethyl chitin beads for oral delivery of protein drugs, *Macromol. Biosci.*, 2005, **5**, 881–889.

70 P. Demianenko, B. Minisini, M. Lamrani and F. Poncin-Epaillard, Stiff IPN hydrogels of poly(acrylamide) and alginate: Influence of the crosslinking ion's valence on hydrogel's final properties, *J. Chem. Eng. Process. Technol.*, 2016, **7**, 4.

71 I. Machida-Sano, M. Hirakawa, H. Matsumoto, M. Kamada, S. Ogawa, N. Satoh and H. Namiki, Surface characteristics determining the cell compatibility of ionically cross-linked alginate gels, *Biomed. Mater.*, 2014, **9**, 025007.

72 Y. Nishio, A. Yamada, K. Ezaki, Y. Miyashita, H. Furukawa and K. Horie, Preparation and magnetometric characterization of iron oxide-containing alginate/poly(vinyl alcohol) networks, *Polymer*, 2004, **45**, 7129–7136.

73 P. V. Finotelli, M. A. Morales, M. H. Rocha-Leao, E. M. Baggio-Saitovitch and A. M. Rossi, Magnetic studies of iron(III) nanoparticles in alginate polymer for drug delivery applications, *Mater. Sci. Eng., C*, 2004, **24**, 625–629.

74 S. H. Ching, N. Bansal and B. Bhandari, Alginate gel particles – A review of production techniques and physical properties, *Crit. Rev. Food Sci. Nutr.*, 2017, **57**, 1133–1152.

75 O. Churio, F. Pizarro and C. Valenzuela, Preparation and characterization of iron-alginate beads with some types of iron used in supplementation and fortification strategies, *Food Hydrocolloids*, 2018, **74**, 1–10.

76 G. Skjåk-Bræk, H. Grasdalen and O. Smidsrød, Inhomogeneous polysaccharide ionic gels, *Carbohydr. Polym.*, 1989, **10**, 31–54.

77 E. S. Chan, B. B. Lee, P. Ravindra and D. Poncelet, Prediction models for shape and size of Ca-alginate macrobeads produced through extrusion-dripping method, *J. Colloid Interface Sci.*, 2009, **338**, 63–72.

78 D. Poncelet, Production of alginate beads by emulsification/internal gelation, *Ann. N. Y. Acad. Sci.*, 2001, **944**, 74–82.

79 K. Liu, H.-J. Ding, J. Liu, Y. Chen and X.-Z. Zhao, Shape-controlled production of biodegradable calcium alginate gel microparticles using a novel microfluidic device, *Langmuir*, 2006, **22**, 9453–9457.

80 V. Bocharova, D. Sharp, A. Jones, S. W. Cheng, P. J. Griffin, A. L. Agapov, D. Voylov, Y. Y. Wang, A. Kisliuk, A. Melman and A. P. Sokolov, Enzyme induced formation of monodisperse hydrogel nanoparticles tunable in size, *Chem. Mater.*, 2015, **27**, 2557–2565.

81 Z. Jin, A. M. Harvey, S. Mailloux, J. Halámek, V. Bocharova, M. R. Twiss and E. Katz, Electrochemically stimulated release of lysozyme from alginate matrix cross-linked with iron cations, *J. Mater. Chem.*, 2012, **22**, 19523–19528.

82 K. I. Draget, K. Østgaard and O. Smidsrød, Homogeneous alginate gels: A technical approach, *Carbohydr. Polym.*, 1991, **14**, 159–178.

83 G. Liu, H. Zhou, H. Wu, R. Chen and S. Guo, Preparation of alginate hydrogels through solution extrusion and the release behavior of different drugs, *J. Biomater. Sci., Polym. Ed.*, 2016, **27**, 1808–1823.

84 M. B. Brunchet, N. L. Mendelson and A. Melman, Photochemical patterning of ionically cross-linked hydrogels, *Processes*, 2013, **1**, 153–166.

85 R. P. Narayanan, G. Melman, N. J. Letourneau, N. L. Mendelson and A. Melman, Photodegradable iron(III) cross-linked alginate gels, *Biomacromolecules*, 2012, **13**, 2465–2471.

86 H. E. Knoop, *Process for solvent casting a film*, US Pat. 4664859, May 12, 1987.



87 Y. Bai, Y. Zhao, Y. Li, J. Xu, X. Fu, X. Gao and Z. Li, UV-Shielding alginate films crosslinked with  $\text{Fe}^{3+}$  containing EDTA, *Carbohydr. Polym.*, 2019, **239**, 115480.

88 X. Wang and H. G. Spencer, Calcium alginate gels: Formation and stability in the presence of an inert electrolyte, *Polymer*, 1998, **39**, 2759–2764.

89 H. Tanaka and S. Irie, Preparation of stable alginate gel beads in electrolyte solutions using  $\text{Ba}^{2+}$  and  $\text{Sr}^{2+}$ , *Biotechnol. Tech.*, 1988, **2**, 115–120.

90 S. Birnbaum, R. Pendleton, P. Larson and K. Mosbach, Covalent stabilization of alginate gel for the entrapment of living whole cells, *Biotechnol. Lett.*, 1981, **3**, 394–400.

91 M. L. Moya, M. Morley, O. Khanna, E. C. Opara and E. M. Brey, Stability of alginate microbead properties in vitro, *J. Mater. Sci.: Mater. Med.*, 2012, **23**, 903–912.

92 Y. Zhuang, F. Yu, H. Chen, J. Zheng, J. Ma and J. Chen, Alginate/graphene double-network nanocomposite hydrogel beads with low-swelling, enhanced mechanical properties, and enhanced adsorption capacity, *J. Mater. Chem. A*, 2016, **4**, 10885–10892.

93 C. Peng, Q. Wang, D. Lu, W. Han and F. Li, A novel bifunctional endolytic alginate lyase with variable alginate-degrading modes and versatile monosaccharide-producing properties, *Front. Microbiol.*, 2018, **9**, 167.

94 T. Y. Wong, L. A. Preston and N. L. Schiller, Alginate lyase: Review of major sources and enzyme characteristics, structure-function analysis, biological roles, and applications, *Annu. Rev. Microbiol.*, 2000, **54**, 289–340.

95 A. Inoue and T. Ojima, Functional identification of alginate lyase from the brown alga *Saccharina japonica*, *Sci. Rep.*, 2019, **9**, 4937.

96 A. H. Badur, S. S. Jagtap, G. Yalamanchili, J.-K. Lee, H. Zhao and C. V. Rao, Alginate lyases from alginate-degrading *Vibrio splendidus* 12B01 are endolytic, *Appl. Environ. Microbiol.*, 2015, **81**, 1865–1873.

97 B. Balakrishnan, S. Lesieur, D. Labarre and A. Jayakrishnan, Periodate oxidation of sodium alginate in water and in ethanol-water mixture: a comparative study, *Carbohydr. Res.*, 2005, **340**, 1425–1429.

98 A. Konwar and D. Chowdhury, Property relationship of alginate and alginate–carbon dot nanocomposites with bivalent and trivalent cross-linker ions, *RSC Adv.*, 2015, **5**, 62864.

99 *Chemistry of Polysaccharides*, ed. G. Zaikov, CRC Press, 2005.

100 Y. Filipov, M. Gamella and E. Katz, Nano-species release system activated by enzyme-based XOR logic gate, *Electroanalysis*, 2017, **29**, 1–7.

101 S. Murdan, Electro-responsive drug delivery from hydrogels, *J. Controlled Release*, 2003, **92**, 1–17.

102 T. Sakai, Osmotic pressure, in *Physics of Polymer Gels*, ed. T. Sakai, Wiley-VCH, Weinheim, 2020, ch. 14.

103 V. Bocharova, O. Zavalov, K. MacVittie, M. A. Arugula, N. V. Guz, M. E. Dokukin, J. Halámková, I. Sokolov, V. Privman and E. Katz, Biochemical logic approach to biomarker-activated drug release, *J. Mater. Chem.*, 2012, **22**, 19709–19717.

104 S. Goldstein, D. Meyerstein and G. Czapski, The Fenton reagents, *Free Radical Biol. Med.*, 1993, **15**, 435–445.

105 O. Smidsrød, A. Haug and B. Larsen, Kinetic studies on the degradation of alginic acid by hydrogen peroxide in the presence of iron salts, *Acta Chem. Scand.*, 1965, **19**, 143–152.

106 A. V. Okhokhonin, S. Domanskyi, Y. Filipov, M. Gamella, A. N. Kozitsina, V. Privman and E. Katz, Biomolecular release from alginate-modified electrode triggered by chemical inputs processed through a biocatalytic cascade – Integration of biomolecular computing and actuation, *Electroanalysis*, 2018, **30**, 426–435.

107 B. Halliwell, M. V. Clement and L. H. Long, Hydrogen peroxide in the human body, *FEBS Lett.*, 2000, **486**, 10–13.

108 H. J. Forman, A. Bernardo and K. J. A. Davies, What is the concentration of hydrogen peroxide in blood and plasma?, *Arch. Biochem. Biophys.*, 2016, **603**, 48–53.

109 J. Pravda, Hydrogen peroxide and disease: towards a unified system of pathogenesis and therapeutics, *Mol. Med.*, 2020, **26**, 41.

110 M. Criado-Gonzalez, L. Corbella, B. Senger, F. Bouldmedais and R. Hernández, Photoresponsive nanometer-scale iron alginate hydrogels: A study of gel–sol transition using a quartz crystal microbalance, *Langmuir*, 2019, **35**, 11397–11405.

111 J. Šima and J. Makáňová, Photochemistry of iron(III) complexes, *Coord. Chem. Rev.*, 1997, **160**, 161–189.

112 J. Chen and R. Browne, Photochemistry of iron complexes, *Coord. Chem. Rev.*, 2018, **374**, 15–35.

113 W. B. Liechty, D. R. Kryscio, B. V. Slaughter and N. A. Peppas, Polymer for drug delivery systems, *Annu. Rev. Chem. Biomol. Eng.*, 2010, **1**, 149–173.

114 R. Narayanaswamy and V. P. Torchilin, Hydrogels and their applications in targeted drug delivery, *Molecules*, 2019, **24**, 603.

115 D. M. Hariyadi and N. Islam, Current status of alginate in drug delivery, *Adv. Pharmacol. Pharm. Sci.*, 2020, 8886095.

116 C. J. Kearney, H. Skaat, S. M. Kennedy, J. Hu, M. Darnell, T. M. Raimondo and D. J. Mooney, Switchable release of entrapped nanoparticles from alginate hydrogels, *Adv. Healthcare Mater.*, 2015, **4**, 1634–1639.

117 J. Zhao, X. Zhao, B. Guo and P. X. Ma, Multifunctional interpenetrating polymer network hydrogels based on methacrylated alginate for the delivery of small molecule drugs and sustained release of protein, *Biomacromolecules*, 2014, **15**, 3246–3252.

118 C. C. Ribeiro, C. C. Barrias and M. A. Barbosa, Calcium phosphate-alginate microspheres as enzyme delivery matrices, *Biomaterials*, 2004, **25**, 4363–4373.

119 M. Shi, H. Zhang, T. Song, X. Liu, Y. Gao, J. Zhou and Y. Li, Sustainable dual release of antibiotic and growth factor from pH-responsive uniform alginate composite microparticles to enhance wound healing, *ACS Appl. Mater. Interfaces*, 2019, **11**, 22730–22744.

120 A. H. E. Machado, D. Lundberg, A. J. Ribeiro, F. J. Veiga, M. G. Miguel, B. Lindman and U. Olsson, Encapsulation of



DNA in macroscopic and nanosized calcium alginate gel particles, *Langmuir*, 2013, **29**, 15926–15935.

121 H. H. Tønnesen and J. Karlsen, Alginate in Drug Delivery Systems, *Drug Dev. Ind. Pharm.*, 2002, **28**, 621–630.

122 V. Pillay, C. M. Dangor, T. Govender, K. R. Moopanar and N. Hurbans, Drug release modulation from cross-linked calcium alginate microdiscs, 1: Evaluation of the concentration dependency of sodium alginate on drug entrapment capacity, morphology, and dissolution rate, *Drug Delivery*, 1998, **5**, 25–34.

123 H. R. Culver, J. R. Clegg and N. A. Peppas, Analyte-responsive hydrogels: Intelligent materials for biosensing and drug delivery, *Acc. Chem. Res.*, 2017, **50**, 170–178.

124 D. H. Camacho, S. J. Y. Uy, M. J. F. Cabrera, M. O. S. Lobregas and T. J. M. C. Fajardo, Encapsulation of folic acid in copper-alginate hydrogels and its slow in vitro release in physiological pH condition, *Food Res. Int.*, 2019, **119**, 15–22.

125 K. I. Draget, G. Skjåk-Bræk and B. T. Stokke, Similarities and differences between alginic acid gels and ionically crosslinked alginate gels, *Food Hydrocolloids*, 2006, **20**, 170–175.

126 M. Gamella, N. Guz and E. Katz, DNA release from a bioelectronic interface stimulated by a DNA signal – Amplification of DNA signals, *Electroanalysis*, 2016, **28**, 2692–2696.

127 D. Massana Roquero, P. Bollella, A. Melman and E. Katz, Nanozyme-triggered DNA release from alginate films, *ACS Appl. Bio Mater.*, 2020, **3**, 3741–3750.

128 V. Privman, S. Domanskyi, R. A. S. Luz, N. Guz, M. G. Glasser and E. Katz, Diffusion of Oligonucleotides from within iron-cross-linked, polyelectrolyte-modified alginate beads: A model system for drug release, *ChemPhysChem*, 2016, **17**, 976–984.

129 *Enzymatic fuel cells: From fundamentals to applications*, ed. P. Atanassov, G. Johnson and H. Luckarift, Wiley-VCH, Weinheim, 2014.

130 M. Gamella, A. Koushanpour and E. Katz, Biofuel Cells – Activation of micro- and macro-electronic devices, *Bioelectrochemistry*, 2018, **119**, 33–42.

131 E. Katz, J. M. Pingarrón, S. Mailloux, N. Guz, M. Gamella, G. Melman and A. Melman, Substance release triggered by biomolecular signals in bioelectronic systems, *J. Phys. Chem. Lett.*, 2015, **6**, 1340–1347.

132 E. Katz, T. Lötzbeyer, D. D. Schlereth, W. Schuhmann and H.-L. Schmidt, Electrocatalytic oxidation of reduced nicotinamide coenzymes at gold and platinum electrode surfaces modified with a monolayer of pyrroloquinoline quinone. Effect of  $\text{Ca}^{2+}$  cations, *J. Electroanal. Chem.*, 1994, **373**, 189–200.

133 S. Mailloux, J. Halámk and E. Katz, A model system for targeted drug release triggered by biomolecular signals logically processed through enzyme logic networks, *Analyst*, 2014, **139**, 982–986.

134 S. Mailloux, K. MacVittie, M. Privman, N. Guz and E. Katz, Starch-powered biofuel cell activated by logically processed biomolecular signals, *ChemElectroChem*, 2014, **1**, 1822–1827.

135 S. Mailloux, Y. V. Gerasimova, N. Guz, D. M. Kolpashchikov and E. Katz, Bridging the two worlds: A universal interface between enzymatic and DNA computing systems, *Angew. Chem., Int. Ed.*, 2015, **54**, 6562–6566.

136 *DNA- and RNA-Based Computing Systems*, E. Katz, Wiley-VCH, Weinheim, 2021.

137 M. Gamella, N. Guz, S. Mailloux, J. M. Pingarrón and E. Katz, Antibacterial drug release electrochemically stimulated by the presence of bacterial cells – Theranostic approach, *Electroanalysis*, 2014, **26**, 2552–2557.

138 S. Mailloux, N. Guz, M. Gamella Carballo, J. M. Pingarrón and E. Katz, Model system for targeted drug release triggered by immune-specific signals, *Anal. Bioanal. Chem.*, 2014, **406**, 4825–4829.

139 I. Willner and E. Katz, Integration of layered redox-proteins and conductive supports for bioelectronic applications, *Angew. Chem., Int. Ed.*, 2000, **39**, 1180–1218.

140 Y. Filipov, P. Bollella and E. Katz, Not-XOR (NXOR) Logic gate realized with enzyme catalyzed reactions: Optical and electrochemical signal transduction, *ChemPhysChem*, 2019, **20**, 2082–2092.

141 M. Gamella, N. Guz, S. Mailloux, J. M. Pingarrón and E. Katz, Activation of a biocatalytic electrode by removing glucose oxidase from the surface – Application to signal triggered drug release, *ACS Appl. Mater. Interfaces*, 2014, **6**, 13349–13354.

142 M. Gamella, N. Guz, J. M. Pingarrón, R. Aslebagh, C. C. Darie and E. Katz, A bioelectronic system for insulin release triggered by ketone body mimicking diabetic ketoacidosis in vitro, *Chem. Commun.*, 2015, **51**, 7618–7621.

143 S. Scheja, S. Domanskyi, M. Gamella, K. L. Wormwood, C. C. Darie, A. Poghossian, M. J. Schöning, A. Melman, V. Privman and E. Katz, Glucose-triggered insulin release from  $\text{Fe}^{3+}$ -cross-linked alginate hydrogel: Experimental study and theoretical modeling, *ChemPhysChem*, 2017, **18**, 1541–1551.

144 M. Gamella, M. Privman, S. Bakshi, A. Melman and E. Katz, DNA release from  $\text{Fe}^{3+}$ -cross-linked alginate films triggered by logically processed biomolecular signals: Integration of biomolecular computing and actuation, *ChemPhysChem*, 2017, **18**, 1811–1821.

145 E. Katz, *Enzyme-Based Computing Systems*, Wiley-VCH, Weinheim, 2019.

146 X. Wang, W. Guo, Y. Hu, J. Wu and H. Wei, *Nanozymes: Next Wave of Artificial Enzymes*, Springer-Verlag, Berlin, Heidelberg, 2016.

147 *Nanozymes – Advances and Applications*, ed. S. Gunasekaran, CRC Press, Boca Raton, FL, 2022.

148 F. Zhou, S. Wu, C. Rader, J. Ma, S. Chen, X. Yuan and E. J. Foster, Crosslinked ionic alginate and cellulose-based hydrogels for photoresponsive drug release systems, *Fibers Polym.*, 2020, **21**, 45–54.

149 G. E. Giannanco, C. T. Sosnofsky and A. D. Ostrowski, Light-responsive iron(III)-polysaccharide coordination hydrogels for controlled delivery, *ACS Appl. Mater. Interfaces*, 2015, **7**, 3068–3076.



150 T. Andersen, P. Auk-Emblem and M. Dornish, 3D Cell culture in alginate hydrogels, *Microarrays*, 2015, **4**, 133–161.

151 I. Machida-Sano, S. Ogawa, H. Ueda, Y. Kimura, N. Satoh and H. Namiki, Effects of composition of iron-cross-linked alginate hydrogels for cultivation of human dermal fibroblasts, *Int. J. Biomater.*, 2012, 820513.

152 I. Machida-Sano, Y. Matsuda and H. Namiki, In vitro adhesion of human dermal fibroblasts on iron cross-linked alginate films, *Biomed. Mater.*, 2009, **4**, 025008.

153 P. A. Underwood and F. A. Bennett, A comparison of the biological activities of the cell-adhesive proteins vitronectin and fibronectin, *J. Cell Sci.*, 1989, **93**, 641–649.

154 I. Machida-Sano, Y. Matsuda and H. Namiki, A novel harvesting method for cultured cells using iron-cross-linked alginate films as culture substrates, *Biotechnol. Appl. Biochem.*, 2010, **55**, 1–8.

155 I. Machida-Sano, S. Ogawa, M. Hirakawa and H. Namiki, Evaluation of three-dimensional porous iron-cross-linked alginate as a scaffold for cell culture, *ISRN Biomater.*, 2014, **2014**, 375758.

156 F. Shuai, Y. Zhang, Y. Yin, H. Zhao and X. Han, Fabrication of an injectable iron(III) crosslinked alginate-hyaluronic acid hydrogel with shear-thinning and antimicrobial activities, *Carbohydr. Polym.*, 2021, **260**, 117777.

157 Y. Amano, P. Qi, Y. Nakagawa, K. Kiritu, S. Ohta and T. Ito, Prevention of peritoneal adhesions by ferric ion-cross-linked hydrogels of hyaluronic acid modified with imino-diacetic acids, *ACS Biomater. Sci. Eng.*, 2018, **4**, 3405–3412.

158 G. E. Giannanco, B. Carrion, R. M. Coleman and A. D. Ostrowski, Photoresponsive polysaccharide-based hydrogels with tunable mechanical properties for cartilage tissue engineering, *ACS Appl. Mater. Interfaces*, 2016, **8**, 14423–14429.

159 J. Zhao, C. Zhou, C. Wu, C. Wu, C. Zhu, C. Ye, S. Wamg and D. Zou, Fe<sup>3+</sup>-Induced synchronous formation of composite hydrogels for effective synergistic tumor therapy in NIR-I/II biowindows, *ACS Appl. Mater. Interfaces*, 2018, **10**, 41947–41955.

160 E. Forgacs, T. Cserháti and G. Oros, Removal of synthetic dyes from wastewaters: A review, *Environ. Int.*, 2004, **30**, 953–971.

161 B. Lellis, C. Z. Fávaro-Polonio, J. A. Paphile and J. C. Polonio, Effects of textile dyes on health and the environment and bioremediation potential of living organisms, *Biotechnol. Res. Innov.*, 2019, **3**, 275–290.

162 S. Hisaindee, M. A. Meetani and M. A. Rauf, Application of LC-MS to the analysis of advanced oxidation process (AOP) degradation of dye products and reaction mechanisms, *Trends Anal. Chem.*, 2013, **49**, 31–44.

163 M. Hartmann, S. Kullmann and H. Keller, Wastewater treatment with heterogeneous Fenton-type catalysts based on porous materials, *J. Mater. Chem.*, 2010, **20**, 9002–9017.

164 H. Zhang, H. J. Choi and C.-P. Huang, Optimization of Fenton process for the treatment of landfill leachate, *J. Hazard. Mater.*, 2005, **125**, 166–174.

165 X. Liu, R. Tang, Q. He, X. Liao and B. Shi, Fe(III)-loaded collagen fiber as a heterogeneous catalyst for the photo-assisted decomposition of Malachite Green, *J. Hazard. Mater.*, 2010, **174**, 687–693.

166 J. Kiwi, N. Denisov, Y. Gak, N. Ovanesyan, P. A. Buffat, E. Suvorova, F. Gostev, A. Titov, O. Sarkisov, P. Albers and V. Nadtochenko, Catalytic Fe<sup>3+</sup> clusters and complexes in Nafion active in photo-Fenton processes. High-resolution electron microscopy and femtosecond studies, *Langmuir*, 2002, **18**, 9054–9066.

167 M. Cheng, W. Song, M. WanHong, C. Chen, J. Zhao, J. Lin and H. Zhu, Catalytic activity of iron species in layered clays for photodegradation of organic dyes under visible irradiation, *Appl. Catal., B*, 2008, **77**, 355–363.

168 J. Fernandez, M. R. Dhananjeyan, J. Kiwi, Y. Senuma and J. Hilborn, Evidence for Fenton photoassisted processes mediated by encapsulated Fe ions at biocompatible pH values, *J. Phys. Chem. B*, 2000, **104**, 5298–5301.

169 G. Ruppert, R. Bauer and G. Heisler, The photo-Fenton reaction – An effective photochemical wastewater treatment process, *J. Photochem. Photobiol., A*, 1993, **73**, 75–78.

170 S. Giannakis, A review of the concepts, recent advances and niche applications of the (photo) Fenton process, beyond water/wastewater treatment: Surface functionalization, biomass treatment, combatting cancer and other medical uses, *Appl. Catal., B*, 2019, **248**, 309–319.

171 A. Fischbacher, C. von Sonntag and T. C. Schmidt, Hydroxyl radical yields in the Fenton process under various pH, ligand concentrations and hydrogen peroxide/Fe(II) ratios, *Chemosphere*, 2017, **182**, 738–744.

172 J. J. Pignatello, E. Oliveros and A. MacKay, Advanced oxidation processes for organic contaminant destruction based on the Fenton reaction and related chemistry, *Crit. Rev. Environ. Sci. Technol.*, 2006, **36**, 1–84.

173 B. Li, Y. Dong, C. Zou and Y. Xu, Iron(III)-alginate fiber complex as a highly effective and stable heterogeneous Fenton photocatalyst for mineralization of organic dye, *Ind. Eng. Chem. Res.*, 2014, **53**, 4199–4206.

174 E. Brillas, I. Sirés and M. A. Oturan, Electro-Fenton process and related electrochemical technologies based on Fenton's reaction chemistry, *Chem. Rev.*, 2009, **109**, 6570–6631.

175 E. Rosales, O. Iglesias, M. Pazos and M. A. Sanromán, Decolourisation of dyes under electro-Fenton process using Fe alginate gel beads, *J. Hazard. Mater.*, 2012, **213–214**, 369–377.

176 O. Iglesias, M. A. Fernández de Dios, E. Rosales, M. Pazos and M. A. Sanromán, Decolourisation and degradation of reactive Black 5 Dye under electro-Fenton process using Fe alginate gel beads, *Environ. Sci. Pollut. Res.*, 2013, **20**, 2172–2183.

177 O. Iglesias, E. Rosales, M. Pazos and M. A. Sanromán, Electro-Fenton decolourisation of dyes in an airlift continuous reactor using iron alginate beads, *Environ. Sci. Pollut. Res.*, 2013, **20**, 2252–2261.

178 D. S. Bezerra, R. J. França and M. R. da Costa Marques, A novel catalytic process for degradation of Bisphenol A in



aqueous solutions using Fe supported on alginate/carboxymethylcellulose, *Catal. Lett.*, 2021, **151**, 1477–1487.

179 T. Rasheed, M. Bilal, F. Nabeel, M. Adeel and H. M. N. Iqbal, Environmentally-related contaminants of high concern: Potential sources and analytical modalities for detection, quantification, and treatment, *Environ. Int.*, 2019, **122**, 52–66.

180 P. Pal, M. Sen, A. Manna, J. Pal, P. Pal, S. Roy and P. Roy, Contamination of groundwater by arsenic: A review of occurrence, causes, impacts, remedies and membrane-based purification, *J. Int. Environ. Appl. Sci.*, 2009, **6**, 295–316.

181 A. Zhitkovich, Chromium in drinking water: Sources, metabolism, and cancer risks, *Chem. Res. Toxicol.*, 2011, **24**, 1617–1629.

182 Y. He, Y. Xiang, Y. Zhou, Y. Yang, J. Zhang, H. Huang, C. Shang, L. Luo, J. Gao and L. Tang, Selenium contamination, consequences and remediation techniques in water and soils: A review, *Environ. Res.*, 2018, **164**, 288–301.

183 D. Mohan, A. Sarswat, Y. S. Ok and C. U. Pittman Jr., Organic and inorganic contaminants removal from water with biochar, a renewable, low cost and sustainable adsorbent – A critical review, *Bioresour. Technol.*, 2014, **160**, 191–202.

184 R. D. Ambashta and M. Sillanpää, Water purification using magnetic assistance: A review, *J. Hazard. Mater.*, 2010, **180**, 38–49.

185 M. M. Khin, A. S. Nair, V. J. Babu, R. Murugan and S. Ramakrishna, A review on nanomaterials for environmental remediation, *Energy Environ. Sci.*, 2012, **5**, 8075–8109.

186 R. Zhu, Q. Chen, Q. Zhou, Y. Xi, J. Zhu and H. He, Adsorbents based on montmorillonite for contaminant removal from water: A review, *Appl. Clay Sci.*, 2016, **123**, 239–258.

187 Q. U. Jiahui, Research progress of novel adsorption processes in water purification: A review, *J. Environ. Sci.*, 2008, **20**, 1–13.

188 P. Rajasulochana and V. Preethy, Comparison on efficiency of various techniques in treatment of waste and sewage water – A comprehensive review, *Resour. – Effic. Technol.*, 2016, **2**, 174–184.

189 S. Rangabhashiyam, E. Suganya, N. Selvaraju and L. A. Varghese, Significance of exploiting non-living biomaterials for the biosorption of wastewater pollutants, *World J. Microbiol. Biotechnol.*, 2014, **30**, 1669–1689.

190 A. K. Vipin, B. Hu and B. Fugetsu, Prussian Blue caged in alginate/calcium beads as adsorbents for removal of cesium ions from contaminated water, *J. Hazard. Mater.*, 2013, **258–259**, 93–101.

191 M. A. De Moraes, D. S. Cocenza, F. C. Vasconcellos, L. F. Fraceto and M. M. Beppu, Chitosan and alginate biopolymer membranes for remediation of contaminated water with herbicides, *J. Environ. Manage.*, 2013, **131**, 222–227.

192 S. F. Lim and J. P. Chen, Synthesis of an innovative calcium-alginate magnetic sorbent for removal of multiple contaminants, *Appl. Surf. Sci.*, 2007, **253**, 5772–5775.

193 J. R. Deans and B. G. Dixon, Uptake of  $Pb^{2+}$  and  $Cu^{2+}$  by novel biopolymers, *Water Res.*, 1992, **26**, 469–472.

194 J. H. Min and J. G. Hering, Arsenate sorption by Fe(III)-doped alginate gels, *Water Res.*, 1998, **32**, 1544–1552.

195 J. H. Min and J. G. Hering, Removal of selenite and chromate using iron(III)-doped alginate gels, *Water Res.*, 1999, **71**, 169–175.

196 M. Xu, T. Zheng, X. Li and X. Dong, Adsorption of Cr(vi) from aqueous solution with double layers calcium-iron-alginate gel beads. 2015, Asia-Pacific Energy Equipment Engineering Research Conference (AP3ER 2015). Proceedings, pp. 210–213.

197 L. Sanaei and M. Tahmasebpoor, Physical appearance and arsenate removal efficiency of Fe(III)-modified clinoptilolite beads affected by alginate-wet-granulation process parameters, *Mater. Chem. Phys.*, 2021, **259**, 124009.

198 M. H. J. S. Karunarathna, R. Hatten, K. M. Bailey, E. T. Lewis, A. L. Morris, A. R. Kolk, J. C. Laib, N. Tembo, R. A. Williams, B. T. Philips, B. L. Ash, W. R. Midden and A. D. Ostrowski, Reclaiming phosphate from waste solutions with Fe(III)-polysaccharide hydrogel beads for photo-controlled-release fertilizer, *J. Agric. Food Chem.*, 2019, **67**, 12155–12163.

199 M. H. J. S. Karunarathna, K. M. Bailey, B. L. Ash, P. G. Matson, H. Wildschutte, T. W. Davis, W. R. Midden and A. D. Ostrowski, Nutrient capture from aqueous waste and photocontrolled fertilizer delivery to tomato plants using Fe(III)-polysaccharide hydrogels, *ACS Omega*, 2020, **5**, 23009–23020.

200 N. Xu, J. Xu, X. Zheng and J. Hui, Preparation of injectable composite hydrogels by blending poloxamers with calcium carbonate-crosslinked sodium alginate, *ChemistryOpen*, 2020, **9**, 451–458.

201 M. T. Cook, G. Tzortzis, V. V. Khutoryanskiy and D. Charalampopoulos, Layer-by-layer coating of alginate matrices with chitosan-alginate for the improved survival and targeted delivery of probiotic bacteria after oral administration, *J. Mater. Chem. B*, 2013, **1**, 52–60.

202 G. Li, T. Gao, G. Fan, Z. Liu, Z. Liu, J. Jiang and Y. Zhao, Photoresponsive shape memory hydrogels for complex deformation and solvent-driven actuation, *ACS Appl. Mater. Interfaces*, 2020, **12**, 6407–6418.

203 Z. Jing, X. Dai, X. Xian, X. Du, M. Liao, P. Hong and Y. Li, Tough, stretchable and compressive alginate-based hydrogels achieved by non-covalent interactions, *RSC Adv.*, 2020, **10**, 23592–23606.

204 R. Hernández and C. Mijangos, In situ synthesis of magnetic iron oxide nanoparticles in thermally responsive alginate-poly(*N*-isopropylacrylamide) semi-interpenetrating polymer networks, *Macromol. Rapid Commun.*, 2009, **30**, 176–181.

205 J. Sun, J. Yu, Z. Jiang, Z. Zhao and Y. Xia, Fluorescent carbonized polymer dots prepared from sodium alginate based on the CEE effect, *ACS Omega*, 2020, **5**, 27514–27521.

206 Y. Li, A. Mohammed, D. Li and L. Wang, Test strips based on iron(III)-impregnated alginate/polyacrylonitrile nanofibers for naked eye screening of tetracycline, *Analyst*, 2018, **143**, 3029–3039.



207 A. V. Singh, T. Gharat, M. Batuwangala, B. W. Park, T. Endlein and M. Sitti, Three-dimensional patterning in biomedicine: Importance and applications in neuropharmacology, *J. Biomed. Mater. Res., Part B*, 2017, **106**, 1369–1382.

208 Z. Nie and E. Kumacheva, Patterning surfaces with functional polymers, *Nat. Mater.*, 2008, **7**, 277–290.

209 B. Chueh, Y. Zheng, Y. Torisawa, A. Y. Hsiao, C. Ge, S. Hsiong, N. Huebsch, R. Franceschi, D. J. Mooney and S. Takayama, Patterning alginate hydrogels using light-directed release of caged calcium in a microfluidic device, *Biomed. Microdevices*, 2010, **12**, 145–151.

210 R. M. Johann and P. Renaud, Microfluidic patterning of alginate hydrogels, *Biointerphases*, 2007, **2**, 73–79.

211 M. Brunchet and A. Melman, Fabrication of patterned calcium cross-linked alginate hydrogel films and coatings through reductive cation exchange, *Carbohydr. Polym.*, 2015, **131**, 57–64.

212 G. E. Giammanco and A. D. Ostrowski, Photopatterning the mechanical properties of polysaccharide-containing gels using  $Fe^{3+}$  coordination, *Chem. Mater.*, 2015, **27**, 4922–4925, see also the ESI.

213 P. J. Bracher, M. Gupta, E. T. Mack and G. M. Whitesides, Heterogeneous films of ionotropic hydrogels fabricated from delivery templates of patterned paper, *ACS Appl. Mater. Interfaces*, 2009, **1**, 1807–1812.

214 *Molecular and Supramolecular Information Processing – From Molecular Switches to Logic Systems*, ed. E. Katz, Wiley-VCH, Weinheim, 2012.

215 *Biomolecular Computing – From Logic Systems to Smart Sensors and Actuators*, ed. E. Katz, Wiley-VCH, Weinheim, 2012.

216 *Advances in Unconventional Computing, in series: Emergence, Complexity and Computation*, ed. A. Adamatzky, Springer, Switzerland, 2017.

217 E. Katz, Boolean logic gates realized with enzyme-catalyzed reactions – Unusual look at usual chemical reactions, *ChemPhysChem*, 2019, **20**, 9–22.

218 E. Katz and V. Privman, Enzyme-based logic systems for information processing, *Chem. Soc. Rev.*, 2010, **39**, 1835–1857.

219 E. Katz and M. Pita, Biofuel cells controlled by logically processed biochemical signals: Towards physiologically regulated bioelectronic devices, *Chem. – Eur. J.*, 2009, **15**, 12554–12564.

220 J. Wang, *Nanomachines: Fundamentals and Applications*, Wiley-VCH, Weinheim, 2013.

221 B. Wang, Y. S. Wan, Y. L. Zheng, X. Q. Lee, T. Z. Liu, Z. B. Yu, J. Huang, Y. S. Ok, J. J. Chen and B. Gao, Alginate-based composites for environmental applications: a critical review, *Rev. Environ. Sci. Bio/Technol.*, 2019, **49**, 318–356.

222 E. Katz, *Signal-Switchable Electrochemical Systems – Materials, Methods, and Applications*, Wiley-VCH, Weinheim, 2018.

223 S. Yin and Z. F. Ma, “Smart” sensing interface for the improvement of electrochemical immunosensor based on enzyme-Fenton reaction triggered destruction of  $Fe^{3+}$  cross-linked alginate hydrogel, *Sens. Actuators, B*, 2019, **281**, 857–863.

224 Y. S. Li, Z. S. Wang, X. Y. Wang, B. Yan, Y. J. Peng and R. Ran,  $Fe^{3+}$ -citric acid/sodium alginate hydrogel: A photo-responsive platform for rapid water purification, *Carbohydr. Polym.*, 2021, **269**, 118269.

225 N. Perez-Moral, M. C. Gonzalez and R. Parker, Preparation of iron-loaded alginate gel beads and their release characteristics under simulated gastrointestinal conditions, *Food Hydrocolloids*, 2013, **31**, 114–120.

226 M. Ergut and A. Ozer, Heterogeneous Fenton-like decolorization of Procion Red MX-5B with iron-alginate gel beads as an effective catalyst, *Tehnicki Glasnik – Technical Journal*, 2019, **13**, 297–304.

227 L. P. Gao, Y. Li, Z. Z. Huang and H. L. Tan, Visual detection of alkaline phosphatase based on ascorbic acid-triggered gel-sol transition of alginate hydrogel, *Anal. Chim. Acta*, 2021, **1148**, 238193.

228 M. Y. Wang, L. Luo, L. H. Fu and H. Yang, Ion responsiveness of polyacrylamide/sodium alginate (PAM/SA) shape memory hydrogel, *Soft Mater.*, 2019, **17**, 418–426.

229 B. Y. Swamy and Y. S. Yun, In vitro release of metformin from iron(III) cross-linked alginate-carboxymethyl cellulose hydrogel beads, *Int. J. Biol. Macromol.*, 2015, **77**, 114–119.

230 R. Hernandez, J. Sacristan and C. Mijangos, Sol/gel transition of aqueous alginate solutions induced by  $Fe^{2+}$  cations, *Macromol. Chem. Phys.*, 2010, **211**, 1254–1260.

231 Y. M. Li and H. H. Liu, Electrochemical behavior of hemoglobin entrapped in sodium alginate hydrogel films, *Chin. J. Anal. Chem.*, 2005, **33**, 843–846.

232 J. V. Alegre-Requena, M. Haring, R. P. Herrera and D. D. Diaz, Regulatory parameters of self-healing alginate hydrogel networks prepared via mussel-inspired dynamic chemistry, *New J. Chem.*, 2016, **40**, 8493–8501.

233 M. Y. Zhou, Q. B. Hu, T. R. Wang, J. Y. Xue and Y. C. Luo, Alginate hydrogel beads as a carrier of low density lipoprotein/pectin nanogels for potential oral delivery applications, *Int. J. Biol. Macromol.*, 2018, **120**, 859–864.

234 O. Iglesias, J. Gomez, M. Pazos and M. A. Sanroman, Electro-Fenton oxidation of imidacloprid by Fe alginate gel beads, *Appl. Catal., B*, 2014, **144**, 416–424.

235 R. Crichton, *Iron Metabolism: From Molecular Mechanisms to Clinical Consequences*, Wiley, Weinheim, 4th edn, 2016.

236 W. E. Winter, L. A. L. Bazydlo and N. S. Harris, The molecular biology of human iron metabolism, *Lab. Med.*, 2014, **45**, 92–102.

